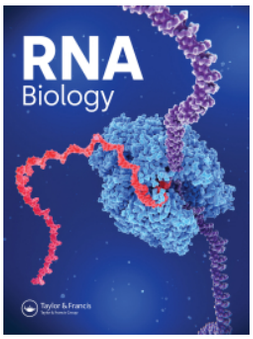

RNA Biology

ISSN: 1547-6286 (Print) 1555-8584 (Online) Journal homepage: www.tandfonline.com/journals/krnb20

Mechanistic insight into the pseudouridylation of RNA

Ting-Yu Lin, Yasmin Stone & Sebastian Glatt

To cite this article: Ting-Yu Lin, Yasmin Stone & Sebastian Glatt (2025) Mechanistic insight into the pseudouridylation of RNA, RNA Biology, 22:1, 1-25, DOI: 10.1080/15476286.2025.2541421

To link to this article: https://doi.org/10.1080/15476286.2025.2541421

© 2025 The Author(s). Published by Informa UK Limited, trading as Taylor & Francis Group.

Published online: 09 Aug 2025.

Submit your article to this journal

Article views: 2785

View related articles

View Crossmark data

Citing articles: 1 View citing articles

Full Terms & Conditions of access and use can be found at
https://www.tandfonline.com/action/journalInformation?journalCode=krnb20

RNA BIOLOGY
2025, VOL. 22, NO. 1, 1–25
https://doi.org/10.1080/15476286.2025.2541421

Taylor & Francis
Taylor & Francis Group

OPEN ACCESS Check for updates

Mechanistic insight into the pseudouridylation of RNA

Ting-Yu Lin[a], Yasmin Stone[a] and Sebastian Glatt[b,c]

[a]Department of Biosciences, Durham University, Durham, UK; [b]Malopolska Centre of Biotechnology, Jagiellonian University, Krakow, Poland; [c]Department of Biological Sciences and Pathobiology, University of Veterinary Medicine Vienna, Vienna, Austria

ABSTRACT

Pseudouridylation (Ψ) is a highly abundant and conserved RNA modification that is present in all three domains of life. The incorporation of Ψ can affect the stability of RNAs, modulate their interaction patterns, and regulate many other aspects of RNA biology. Ψ are introduced by a structurally highly related enzyme family, called pseudouridine synthases (PUS). Each PUS enzyme targets distinct RNA substrates and target sites. Dysregulation of PUS enzymes has been implicated in neurodevelopmental disorders, mitochondrial diseases and cancer. These clinical consequences highlight the ultimate need to understand how these enzymes catalyze their modification reactions and achieve target selectivity as well as specificity. In this review, we summarize the currently available structural information on PUS enzymes and highlight the most recent progress in understanding some underlying mechanistic principles. Furthermore, we illustrate the increasing therapeutic applications related to the so-called 5th RNA base.

ARTICLE HISTORY
Revised 27 June 2025
Accepted 25 July 2025

KEYWORDS
Pseudouridine; tRNA; RNA modification; pseudouridine synthase; cryo-electron microscopy; crystallography; neurodegenerative disease; cancer

Introduction

RNA has traditionally been recognized as a messenger molecule that transfers information from DNA to proteins. However, RNA plays a far more dynamic role in cellular regulation due to its structural and functional versatility. This versatility is largely driven by RNA modifications, with over 170 distinct chemical modifications identified across RNA bases, sugars, and backbones [1]. The post-transcriptional incorporation of those modifications contributes to RNA stability, molecular interactions, and regulatory functions, influencing the majority of cellular processes [2]. Increasing evidence links dysregulated RNA modifications to human diseases and other pathogenic consequences, underscoring their biological importance [3].

Among these RNA modifications, pseudouridylation (Ψ) is universally conserved across all domains of life. This modification involves the isomerization of uridine, converting the carbon-nitrogen glycosidic bond (C1′-N1) into a carbon–carbon (C1-C5) bond, which is the hallmark of pseudouridine [4]. This structural rearrangement creates an additional N1-H donor at the Hoogsteen edge, providing an additional opportunity for the formation of a hydrogen bond, enhancing RNA stability and molecular interactions. Advances in high-throughput pseudouridine detection technologies (e.g. Oxford Nanopore direct RNA sequencing [5], CMC-coupled mass spectrometry [6,7], pseudouridine sequencing (Pseudo-seq) [8], bisulphite-induced deletion sequencing (BID-seq) [9], HydraPsiSeq [10], antibody-based Ψ identification [11], RT-PCR-based Ψ identification [12], or 2-bromoacrylamide-assisted cyclization sequencing (BACS) [13] have expanded our understanding of pseudouridine landscapes [14] in coding and non-coding RNAs *in vivo* (for details see excellent reviews [15–21]. Notably, pseudouridylation has been recognized as both, a constitutive and dynamic modification, responding to internal or external stimuli to modulate RNA function [22–24]. One key functional advantage of pseudouridine incorporation appears to be an increased RNA stability, contributing to the turnover and half-life time of the transcriptome and translatome [25]. Notably, tRNA is a class of RNA with highly conserved pseudouridylation sites, including Ψ_{13}, $\Psi_{27/28}$, $\Psi_{38/39/40}$, Ψ_{54}, and Ψ_{55}. However, not all tRNAs contain the same number of Ψs. Interestingly, each Ψ-site contributes differently to the stability of individual tRNAs, suggesting that RNA modifications may have

CONTACT Ting-Yu Lin ting-yu.lin@durham.ac.uk Department of Biosciences, Durham University, Durham DH1 3LE, UK; Sebastian Glatt sebastian.glatt@uj.edu.pl Malopolska Centre of Biotechnology, Jagiellonian University, Krakow 30-387, Poland

© 2025 The Author(s). Published by Informa UK Limited, trading as Taylor & Francis Group.
This is an Open Access article distributed under the terms of the Creative Commons Attribution-NonCommercial License (http://creativecommons.org/licenses/by-nc/4.0/), which permits unrestricted non-commercial use, distribution, and reproduction in any medium, provided the original work is properly cited. The terms on which this article has been published allow the posting of the Accepted Manuscript in a repository by the author(s) or with their consent.

site-specific regulatory effects on tRNA function [26]. In ribosomal RNAs (rRNA) Ψs are found at several conserved sites [27] and they particularly contribute to ribosomal biogenesis and maturation [28]. In general, incorporating Ψs in RNAs seems to stabilize the structure of folded regions, but in a few cases Ψs could directly (or indirectly) attenuate RNA-protein interactions [29]. A recent study combining molecular dynamics (MD) simulation with comprehensive biophysical analyses on the contribution of individual Ψs to the stability of tRNAs, demonstrated that Ψ can enhance the local stability of RNA by promoting the water-mediated interaction with neighbouring nucleotides [26]. Whether the same principle is also responsible for functional effects of Ψs in the context of all RNA molecules and for regulating the interaction with proteins needs to be confirmed in the future.

Pseudouridine synthases (also known as PUS enzymes) catalyze the formation of Ψ and can be classified into six evolutionarily conserved superfamilies: TruA, TruB, TruD, RluA, RsuA, and Pus10 [30,31]. All PUS enzymes show little sequence identity but share a highly conserved fold of the catalytic core, consisting of a mixed α/β topology with antiparallel β-sheets, α-helices, and multiple loops. A few conserved motifs have been identified, which are responsible for RNA binding across most PUS enzymes [32]. In contrast, various additional accessory domains are found in each family members that assist RNA binding and recognition, contributing to high selectivity towards specific set of RNA targets [17], strongly suggesting the necessity of preserving individual PUS family throughout evolution [30,33]. These enzymes function through two distinct mechanisms, namely as (i) stand-alone enzymes or as (ii) RNA guide-dependent H/ACA small ribonucleoproteins (H/ACA RNPs) and the dyskerin (DKC1) complex. First insights into the detailed catalytic mechanism of Ψ-formation appeared, when a Michael addition mechanism was proposed after TruA was shown to form a covalent adduct with 5-fluorouridine (5-FU) [4,34–36]. However, this mechanism does not seem to apply to TruB, which instead operates via an acylal mechanism [37], more precisely a glycal mechanism [34]. This has been supported by kinetic isotope experiments and molecular dynamic simulations in several PUS enzymes, including TruB [38], RluA [32] and DKC1 [39]. In principle, the glycal mechanism could also explain the reaction catalysed by TruA [34], suggesting that may be a general mechanism among diverse PUS enzymes. In brief, PUS enzymes utilizes a highly conserved catalytic aspartic acid residue to deproteinize the C2′ position of the ribose, triggering cleavage of the bond between uracil and ribose. This is followed by a 180° rotation of the base and formation of a new C-C bond to attach the rotated base back to the ribose. While the surrounding amino acids of the active sites need to be involved in catalysis, they often vary among PUS family members and the sequence conservation is surprisingly low [40–42]. As researchers continue to expand the landscapes of pseudouridylation patterns across diverse RNA classes, elucidating the structural and biochemical mechanisms of PUS enzymes remains a critical frontier.

Here, we aim to discuss recent advancements in understanding the underlying catalytic mechanisms of pseudouridylation from the perspective of enzyme mode of action, principles of substrate recognition and the emerging link between mutations in PUS enzymes and human diseases.

Strategy of determining substrate selectivity

As mentioned above, each PUS enzyme appears to have evolved for modifying a distinct RNA target or set of RNA targets [17], and certain Ψ-sites are found within some reoccurring RNA motifs [9,43]. While all PUS enzymes share a highly conserved core topology, it has been speculated that their ability to recognize diverse RNA targets is largely dictated by unique accessory domains that flank the core region [40]. Most PUS are stand-alone enzymes, which catalyze the pseudouridylation on RNA without additional protein or RNA partners [32,42,44,45]. In contrast, DKC1 targets its RNAs through an RNA guide-dependent mechanism, relying on H/ACA small nucleolar RNAs (snoRNAs) to provide precise positional information by complementary sequences to select the target sites [46,47]. Most RNA-bound PUS structures have been resolved using short RNA fragments (Table 1), such as stem loops or single-stranded RNA substrates [32,36,45,48–50]. Among the few exceptions, bacterial TruA has been crystallized with a full-length tRNA [45], while human PUS3, a homolog of bacterial TruA, has recently been resolved by single particle cryo-electron microscopy (cryo-EM) in a complex with tRNA or pre-tRNA, providing comprehensive insights into its recognition mechanism [40]. Here, we will discuss the available structural knowledge (Table 1) about each PUS superfamily, focusing on how their distinct modes of action influence RNA recognition and enzymatic function.

Table 1. Available structures of PUS enzymes with and without bound RNA.

Superfamily	PUS enzyme	status	PDB	Method	resolution
TruA	*E.coli* TruA	apo	1DJ0	X-ray diffraction	1.5 Å
	T. thermophilus HB8 TruA	apo	1VS3	X-ray diffraction	2.25 Å
	H. sapiens PUS1	apo	4J37	X-ray diffraction	1.75 Å
	H. sapiens PUS1	apo	4IQM	X-ray diffraction	1.8 Å
	P. furiosus TruA	apo	8Q70	X-ray diffraction	1.85 Å
	H. sapiens PUS3	apo	9F9Q	cryo-EM	6.5 Å
	E. coli TruA	2 bound tRNAs	2NRE	X-ray diffraction	4 Å
	E. coli TruA	1 bound tRNA	2NQP	X-ray diffraction	3.5 Å
	E. coli TruA	2 bound tRNAs	2NR0	X-ray diffraction	3.9 Å
	S. cerevisiae Pus1	1 bound 5-FU RNA	7R9F	X-ray diffraction	2.89 Å
	S. cerevisiae Pus1	1 bound RNA	7R9G	X-ray diffraction	2.4 Å
	H. sapiens PUS3	2 bound tRNAs	8OKD	cryo-EM	3.1 Å
	H. sapiens PUS3	2 bound tRNAs	9ENE	cryo-EM	3.15 Å
	H. sapiens PUS3	2 bound pre-tRNAs	9ENF	cryo-EM	2.97 Å
	H. sapiens PUS3	2 bound tRNAs	9ENB	cryo-EM	2.66 Å
	H. sapiens PUS3	1 bound tRNA	9ENC	cryo-EM	3.36 Å
TruB	*M. tuberculosis* H37Rv TruB	apo	1SGV	X-ray diffraction	1.9 Å
	T. maritima TruB	apo	1ZE1	X-ray diffraction	2.9 Å
	T. maritima TruB	apo	1R3F	X-ray diffraction	1.85 Å
	H. sapiens TRUB1	apo	8JFX	X-ray diffraction	2.2 Å
	P. furiosus Cbf5	Cbf5-Nop10-Gar1 Complex	2EY4	X-ray diffraction	2.11 Å
	M. jannaschii Cbf5	Cbf5 Nop10 Complex	2APO	X-ray diffraction	1.95 Å
	P. furiosus Cbf5	Cbf5-Nop10-Gar1-snoRNA Complex	2HVY	X-ray diffraction	2.3 Å
	P. abyssi Cbf5	Cbf5-Nop10 Complex	2AUS	X-ray diffraction	2.1 Å
	S. cerevisiae S288C Cbf5	Cbf5-Nop10-Gar1 complex	3U28	X-ray diffraction	1.9 Å
	S. cerevisiae S288C Cbf6	Shq1-Cbf5-Nop10-Gar1 complex	3UAI	X-ray diffraction	3.06 Å
	H. sapiens DKC1	telomerase holoenzyme	7V9A	cryo-EM	3.94 Å
	H. sapiens DKC1	telomerase holoenzyme	7BGB	cryo-EM	3.4 Å
	H. sapiens DKC1	telomerase holoenzyme	8OUE	cryo-EM	2.7 Å
	H. sapiens DKC1	telomerase holoenzyme	8OUF	cryo-EM	2.7 Å
	T. maritima TruB	RNA hairpin	1ZE2	X-ray diffraction	3.0 Å
	T. maritima TruB	RNA hairpin	1R3E	X-ray diffraction	2.1 Å
	T. maritima TruB	RNA hairpin	2AB4	X-ray diffraction	2.4 Å
	E. coli TruB	RNA hairpin	1K8W	X-ray diffraction	1.85 Å
	E. coli TruB	RNA hairpin	1ZL3	X-ray diffraction	2.8 Å
	P. furiosus Cbf5	Cbf5-Nop10-Gar1-snoRNA-target RNA Complex	2RFK	X-ray diffraction	2.87 Å
	P. furiosus Cbf5	Cbf5-Nop10-Gar1-snoRNA-target RNA Complex	3MQK	X-ray diffraction	2.80 Å
	P. furiosus Cbf5	Cbf5-Nop10-L7ae-snoRNA-target RNA (5BrU) Complex	3LWO	X-ray diffraction	2.80 Å
	P. furiosus Cbf5	Cbf5-Nop10-L7ae-snoRNA-target RNA (5BrU) Complex	3LWP	X-ray diffraction	2.50 Å

(*Continued*)

Table 1. (Continued).

Superfamily	PUS enzyme	status	PDB	Method	resolution
	P. furiosus Cbf5	Cbf5-Nop10-L7ae-snoRNA-target RNA (3MU) Complex	3LWQ	X-ray diffraction	2.68 Å
	P. furiosus Cbf5	Cbf5-Nop10-L7ae-snoRNA-target RNA (4SU) Complex	3LWR	X-ray diffraction	2.20 Å
	P. furiosus Cbf5	Cbf5-Nop10-L7ae-snoRNA-target RNA (2′−deoxyuridine) Complex	3LWV	X-ray diffraction	2.50 Å
	P. furiosus Cbf5	Cbf5-Nop10-L7ae-snoRNA-target RNA (FU) Complex	3HAX	X-ray diffraction	2.11 Å
	P. furiosus Cbf5	Cbf5-Nop10-Gar1-L7ae-snoRNA-target RNA (FU) Complex	3HAY	X-ray diffraction	4.99 Å
	P. furiosus Cbf5	Cbf5-Nop10-snoRNA-target RNA (FU) Complex	3HJY	X-ray diffraction	3.65 Å
	P. furiosus Cbf5	Cbf5-Nop10-L7ae-snoRNA-target RNA (FU) Complex	3HJW	X-ray diffraction	2.35 Å
TruD	*E.coli* TruD	apo	1SZW	X-ray diffraction	2.0 Å
	E.coli TruD	apo	1SI7	X-ray diffraction	2.2 Å
	E.coli TruD	apo	1SB7	X-ray diffraction	2.2 Å
	M. mazei TruD	apo	1Z2Z	X-ray diffraction	2.6 Å
	H. sapiens PUS7	apo	5KKP	X-ray diffraction	2.26 Å
	S. cerevisiae PUS7	apo	7MZV	X-ray diffraction	3.2 Å
PUS10	*H. sapiens* PUS10	apo	2V9K	X-ray diffraction	2.0 Å
RluA	*E. coli* RluC	apo	1V9K	X-ray diffraction	2.0 Å
	E. coli RluC	apo	1XPI	X-ray diffraction	2.2 Å
	E. coli RluD	apo	1V9F	X-ray diffraction	1.7 Å
	E. coli RluD	apo	1QYU	X-ray diffraction	2.0 Å
	E. coli RluD	apo	1PRZ	X-ray diffraction	1.8 Å
	E. coli RluD	apo	2IST	X-ray diffraction	1.86 Å
	H. sapiens RPUSD1	apo	5VBB	X-ray diffraction	1.94 Å
	H. sapiens RPUSD4	apo	5UBA	X-ray diffraction	1.54 Å
	E. coli RluA	RNA hairpin	2I82	X-ray diffraction	2.05 Å
RsuA	*H. influenzae* RsuA	apo	1VIO	X-ray diffraction	1.59 Å
	E. coli RsuA	apo	1KSL	X-ray diffraction	2.1 Å
	E. coli RsuA	apo	1KSK	X-ray diffraction	2.0 Å
	E. coli RsuA	apo	1KSV	X-ray diffraction	2.65 Å
	E. coli RluB	apo	4LAB	X-ray diffraction	2.5 Å
	E. coli RluE	apo	2OML	X-ray diffraction	1.2 Å
	E. coli RluE	apo	2OLW	X-ray diffraction	1.6 Å
	E. coli RluF	apo	2GML	X-ray diffraction	2.6 Å
	E. coli RluB	with rRNA	9CL9	cryo-EM	5.04 Å
	E. coli RluB	RNA hairpin	4LGT	X-ray diffraction	1.3 Å
	E. coli RluF	RNA hairpin	3DH3	X-ray diffraction	3.0 Å

PUS3 has a unique homodimer architecture and restricts substrate specificity to tRNAs

The TruA family, which includes PUS1 and PUS3, is conserved in all three domains of life and is known to modify tRNAs [40,51–53]. The crystal structure of bacterial TruA revealed a homodimeric architecture with two-fold symmetry, characteristic of its catalytic conformation (Figure 1) [35,51]. The core domain of TruA exhibits a canonical PUS-fold, including the highly conserved catalytic aspartate residue [51]. Its human counterpart, PUS3, adopts a similar overall homo-dimeric architecure [40,54], but using a completely different dimerization interface. In detail, bacterial TruA relies on loop regions on the top of the core to mediate head-to-head interactions [35]. TruA from *Salmonella enterica* exhibits an even more dynamic dimerization mechanism, assembling into a homodimer only in the presence of tRNA [55]. In contrast, a crystal structure of an archaeal Pus3 [56] and the cryo-EM structure of human PUS3 [40] show that the homo-dimeric structure is formed via an anti-parallel coiled-coil domain via a long C-terminal helix. This domain contains hydrophobic residues that stabilize the interface, allowing dimerization via a different structural mechanism than bacterial TruA.

TruA typically catalyzes pseudouridylation at positions 38, 39 or 40 of tRNA [45], which partially explains the presence of a wide catalytic cleft in TruA, potentially enabling a less stringent positioning of the substrates (Figure 2A). Due to the structural symmetry of the TruA dimer, TruA can accommodate two tRNA molecules simultaneously [45]. Despite the different dimer interface, the binding of two tRNAs has also been observed in human PUS3 [40]. Both enzymes use their dimeric scaffold [40,45] to establish two specific contact points: one monomer binds the tRNA elbow at the G_{19}:C_{56} pair, while the other monomer positions the anticodon stem loop within the catalytic site [40,45]. Of note, mature as well as precursor tRNA (containing an intronic sequence in the anticodon stem) can bind to PUS3 in a similar way [40]. Therefore, it was proposed that the non-catalytic contact site serves as a molecular ruler, ensuring proper tRNA positioning for catalysis [45]. Apart from these two primary contact sites, no additional interactions have been observed between PUS enzymes and the tRNA (e.g. variable loop) [40]. In addition, the L-shaped structure of tRNA remains almost unchanged when binding to TruA or PUS3, showing no major structural rearrangements induced by tRNA binding [40,45]. All of these structures apparently captured a pre-catalytic conformation, where U_{39} remains paired with G_{31} and stacked inside the anticodon stem loop. However, the determined cryo-EM structures of the PUS3-tRNA complex highlight that the anticodon stem-loop (ASL) region remain flexible when bound to PUS3 [40]. Moreover, human PUS3 exhibits strict substrate selectivity towards tRNA-shaped molecules by recognition of their overall architecture, as PUS3 does not bind anticodon stem loops [40]. This specificity was further supported by Pseudo-seq analyses in PUS3-depleted human cells, where no PUS3-dependent Ψ sites could be identified in mRNAs. Similarly, recent bacterial transcriptome analyses did not detect TruA-dependent pseudouridine modifications in mRNAs, suggesting that TruA, like PUS3, might exclusively act on tRNA substrates [25,57].

PUS1 exists as a monomer and recognizes tRnas as well as other RNAs

Human PUS1 also belongs to the TruA superfamily, sharing 37% sequence similarity and 25% identity to human PUS3. Interestingly, these highly related enzymes exhibit distinct substrate preferences and RNA recognition modes [40]. Structurally, PUS1 and PUS3 have conserved core domains, but their C-terminal extensions display several differences and PUS1 [58] seems to completely lacks a C-terminal helix that mediates dimerization in PUS3. In PUS1, this region extends from the back to the top of the enzyme, forming a so-called 'substrate-binding wall' [58], preventing the formation of an RNA binding channel from the catalytic cleft to the outer surface. This unique topology likely accounts for the monomeric state of PUS1 [40] and may drive its distinct substrate preferences (Figure 1). PUS1 modifies uridines residing in the ASL of tRNAs at position 27 and 28. Molecular docking approaches suggest that tRNA binds to human PUS1 in a different orientation than to bacterial TruA [58] and human PUS3 [40]. This difference is likely caused by the topology of the PUS1-specific C-terminal extension, which forms a structural barrier that prevents tRNA from binding in the same manner as observed with dimeric TruA homologs. These findings further emphasize how the structure of PUS enzymes dictates substrate recognition [58]. Unlike PUS3, which seems to exclusively modify tRNA, PUS1 can interact with various RNA molecules, including tRNA and hairpins structures with different

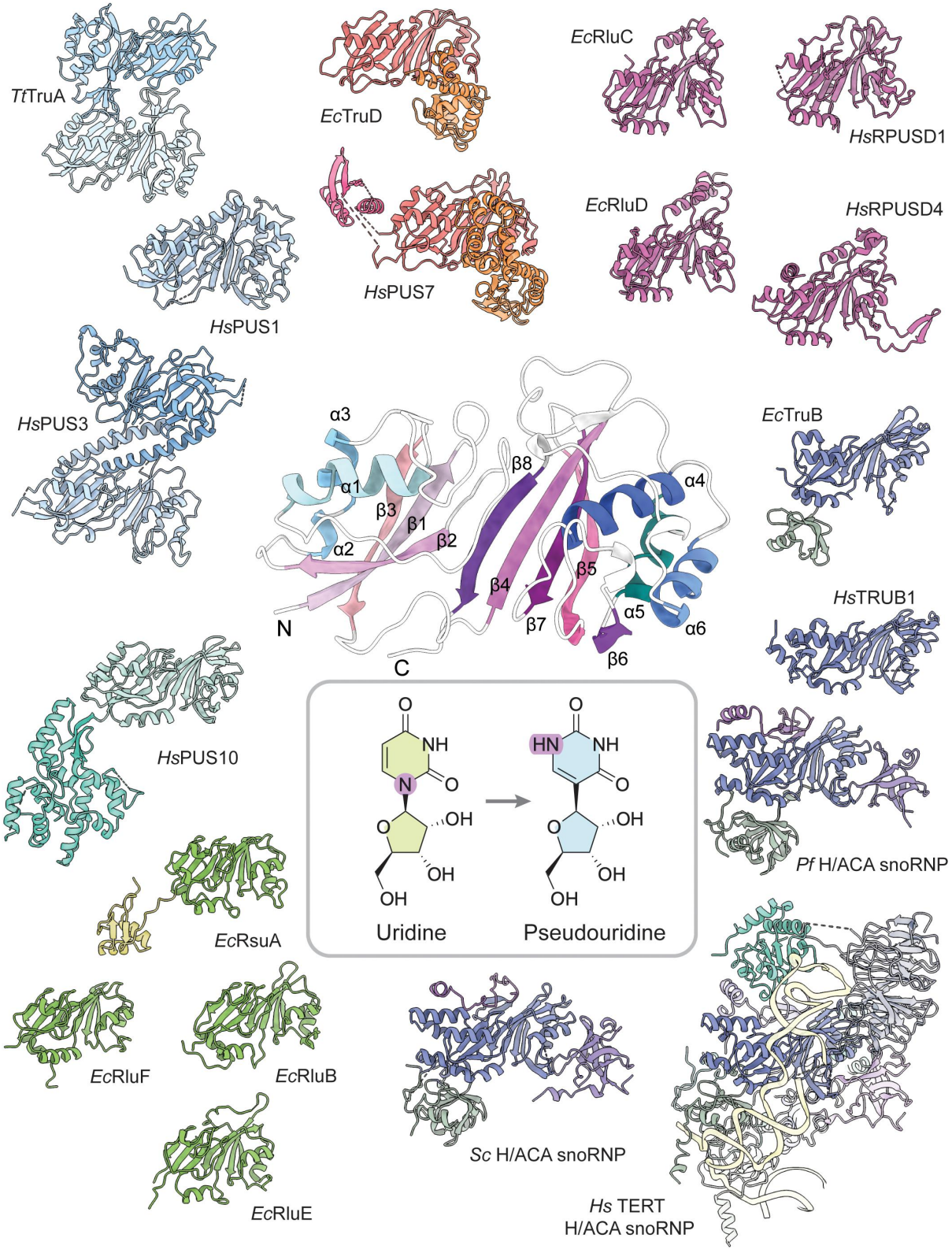

Figure 1. Structure gallery of apo PUS across three domains of life. The cartoon representation of the conserved catalytic core topology and the chemical structures of uridine and pseudouridine are shown in the centre. Secondary structures are highlighted and N- and C- termini are indicated. All six PUS superfamilies are shown in cartoon with ribbon style. Eash superfamily is colored coded at its core region, including light blue for TruA (*Thermus thermophilus* HB8 TruA, 1VS3; *Homo sapiens* PUS1, 4J37; H. sapiens PUS3, 9F9Q), rose for TruD (*Escherichia coli* TruD, 1SZW; *H. sapiens* PUS7, 5KKP), purple for RluA (*E. coli* RluC, 1V9K; *E. coli* RluD, 1QYU; *H. sapiens* RPUSD1, 5VBB; *H. sapiens* RPUSD4, 5UBA), blue for TruB (*E. coli* TruB. 1SGV; *H. sapiens* TRUB1, 8JFX; *Pyrococcus furiosus* Cbf5, 2EY4; *Saccharomyces. cerevisiae* Cbf5, 3U28; *H. sapiens* DKC1, 7RTC),

sequences [40,48]. Hence, PUS1 also displays a broader range of substrate and can introduce Ψ into mRNA, tRNAs and other non-coding RNAs [48]. Although a structure of full length PUS1 bound to a tRNA is still missing, the co-crystal structure of truncated yeast Pus1 in complex with a minimal mRNA substrate provides very useful structural insights (Figure 2A) [48]. The co-crystal structure shows that PUS1 appears to have a larger interaction interface with the RNA than PUS3, involving 13 amino acids to bind RNA bases and the phosphate backbone [48]. While some of these residues are conserved and catalytically important, others are not part of the catalytic site or do not seem to be involved in securing substrate binding, suggesting a role in target selectivity [48]. Furthermore, it has been suggested that PUS1 might recognize a specific motif [59]. Based on computational analyses and mutagenesis, a motif called H-R-U ('H' = adenine/cytosine/thymine; 'R' = guanine/adenine) was identified, which is located at positions −2, −1, and + 1, near the base of a 13-base pair stem-loop structure, containing a small internal bulge [59]. Although 5-FU was also incorporated into the RNA substrate to trap the conformation of a reaction intermediate, the low occupancy of the catalytic site in the crystal structure hindered to obtain detailed insights into the enzymatic reaction mechanism [48].

PUS4/TRUB1 recognizes both, consensus sequence and secondary structure

The TruB superfamily only exists in bacteria and eukarya. Bacterial TruB, called PUS4 in yeast and TRUB1 in humans, harbours a conserved catalytic core domain (with 11 predominantly antiparallel β-strands) at the N-terminus followed by a C-terminal spherical domain (a four-stranded β-sheet and a single helix). TruB is responsible for the formation of Ψ_{55}, which is almost universal found in mitochondrial and cytosolic tRNAs, except for the initiator $tRNA^{Met}$ (Figure 2A) [60–62]. The U_{55}-target always pairs with G_{18} and is located in the TΨC-arm of tRNA that is in proximity of the tRNA 'elbow', formed by the reverse Hoogsteen base pair (U_{54} pairing with A_{58}) and seven canonical 'Watson-Crick' base pairs. Several crystal structures of bacterial TruB proteins are available (Table 1), including RNA-bound complexes [36,44]. The initial TruB-RNA complex was derived from co-crystal structures of bacterial TruB with a short RNA stem loop, mimicking a tRNA T-arm [36,44]. The core structure of the enzyme remains mostly unchanged after RNA binding and accommodation. However, several RNA binding loops become structured or significant change their position in the RNA-bound complex, when compared to the apo structure [44]. The TruB-RNA co-crystal structure shows that U_{55} is flipped out and is positioned within the catalytic site, whereas the rest of the RNA mostly remains in its original conformation [36]. As the N-terminal domain of TruB largely covers the RNA interaction area, docking of a full length tRNA molecule suggests that the C-terminal domain of TruB contacts the acceptor stem. Although no structure information with a full length tRNA is available at the moment, the binding affinities of TruB towards the T-arm mimetic and full length tRNA are in a similar range. Hence, the pre-folded stem-loop of the T-arm can serve as a structural model for recognition by TruB through shape complementarity [36,60,63]. In addition, the sequence motif of the used stem loop is crucial for the recognition requirement, namely G_{53}, U_{54}, U_{55}, A_{58}, C_{61}, and a preference for C at position 56 [36,63]. This additional sequence dependency also explains why initiator $tRNA^{Met}$ is not a substrate of TruB, as it lacks the U_{54}:A_{58} base pair. In contrast to the well-characterized bacterial TruB, our understanding of eukaryotic TruB homologs (e.g. PUS4/TRUB1) remains limited. Although a crystal structure of human PUS4 has been reported (Table 1), it only contains the highly conserved core domain (Figure 1). The absence of structural information on the full-length protein (including accessory domains) and its complex with a RNA substrate leaves a uncertainty whether eukaryotic PUS4 recognizes substrates in a similar fashion as its bacterial counterpart(s). Further structural and functional studies will be needed to elucidate the molecular basis of RNA recognition by PUS4/TRUB1.

Despite the lack of structural information on eukaryotic PUS4/TRUB1 enzymes, functional studies on the pseudouridylation on tRNAs [64,65], mitochondrial tRNAs [62] and mRNAs [8,43] have been carried

green for RsuA (*E. coli* RsuA, 1KSL; *E. coli* RluB, 4LAB; *E. coli* RluF, 2OML; *E. coli* RluE, 2GML), light cyan for Pus10 (*H. sapiens* PUS10, 2V9K). The accessory domains or subunits are colored with similar color scheme. Human TERT H/ACA snoRNAP has a guide RNA bound, which is highlighted in light yellow.

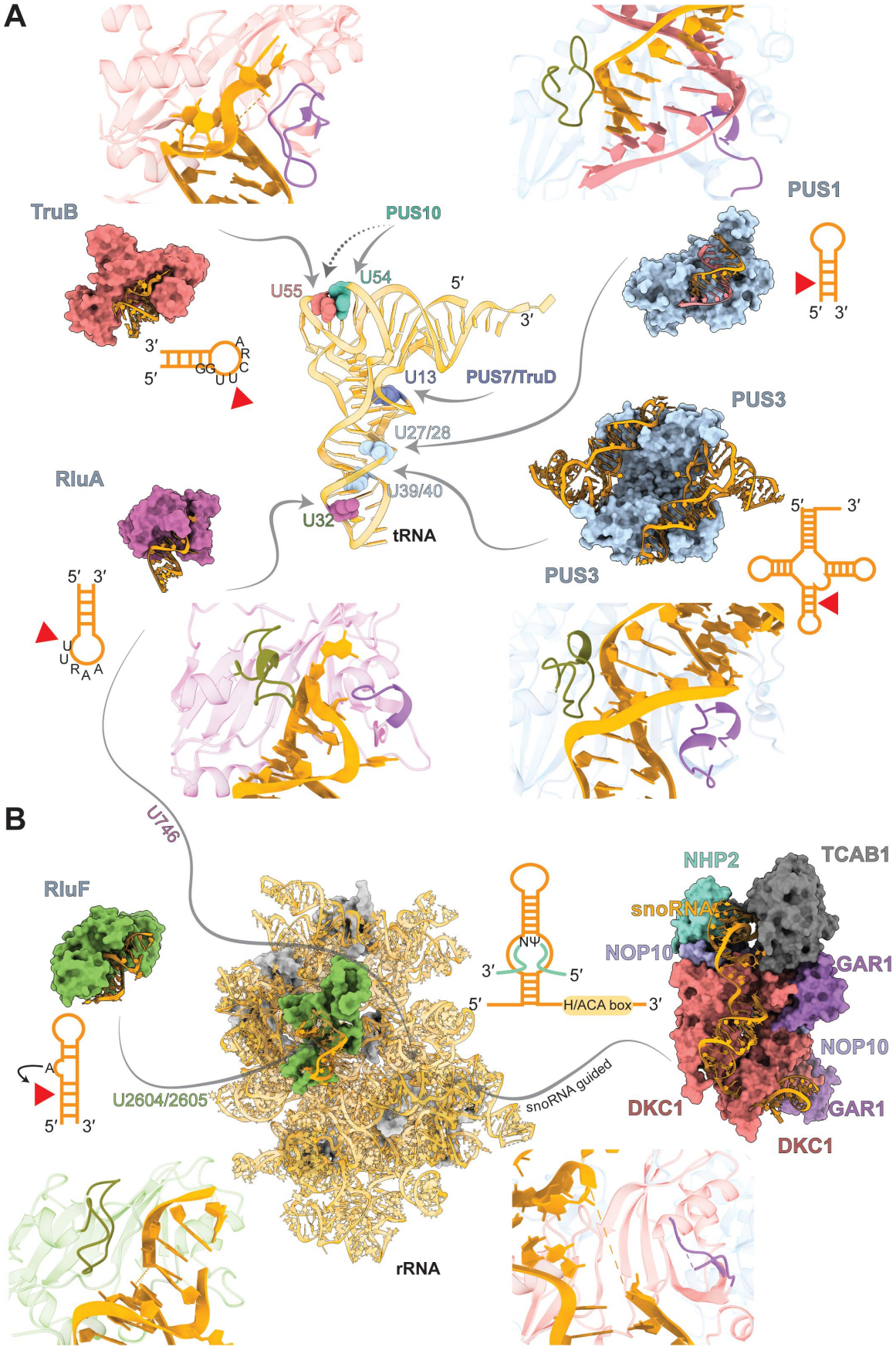

Figure 2. Structure gallery of RNA bound PUS. (A). A cartoon representative of a tRNA molecule (1EHZ) in the centre with Ψ sites highlighted in balls. Representatives of RNA bound PUS are shown where PUS is displayed with surface and RNA is with

out. Hence, it seems certain that the eukaryotic PUS4/TRUB1 is catalytically highly similar to its bacterial homologs, converting U_{55} to Ψ_{55} in tRNAs. Moreover, based on transcriptome-wide pseudouridine profiling analyses, PUS4/TRUB1 can introduce Ψs in mRNAs [9,43,66], where the targeted sites resides in a GUΨCNANNC consensus sequence motif [8]. However, no experimental evidence confirms whether the structure of these non-tRNA target sites is still crucial for PUS4/TRUB1 recognition. A recent study that analyzed the bacterial transcriptome by pseudouridine profiling shows a cluster of Ψs at the TruB recognition motif [25]. However, additional validation studies will still be required to confirm that bacterial TruB also acts on coding RNAs, like its eukaryotic homologs.

PUS7 displays a multisite – multisubstrate modification activity

PUS7 is a member of the TruD superfamily and is conserved across all three domains of life [67]. Several crystal structures of apo PUS7 homologs revealed a characteristic V-shaped architecture (Figure 1) [42,68–70]. The protein family contains a spherical TruD domain at the N-terminus, followed by a conserved core domain that adopts a topology similar to other PUS enzymes. These domains are connected via a loop-rich region. The TruD domain, a hallmark of the TruD superfamily, contains two conserved motifs (residues 155–169 and 196–211 in *E. coli* TruD) that may contribute to tRNA binding [42,69,71]. The human PUS7 structure further exhibits two inserted subdomains, including an R3H-like domain (residues 162–236) and insertion C (residues 381–578) [68]. R3H-like domains are known nucleic acid-binding domains, which likely expands the RNA-binding interface [68] and promotes RNA substrate interaction.

Although no structure of a PUS7–RNA complex has been resolved yet, comprehensive biochemical studies suggest that PUS7 is one of the most versatile stand-alone PUS enzymes [68]. In detail, PUS7 seems to be capable of modifying multiple RNA classes by recognizing both, secondary structure elements as well as specific consensus sequences. PUS7 is known to catalyze Ψ_{13} in tRNA and Ψ_{35} in pre-$tRNA^{Tyr}$, which are conserved across many species, including humans [67,72,73]. These pseudouridylation sites are embedded within a conserved seven-nucleotide motif, Pu(G/C)UNΨAPu, where 'Pu' represents purines and N can represents any nucleotide [72]. This consensus sequence is phylogenetically conserved across tRNAs from most organisms, but is missing in archaea [42]. Moreover, the local structure formed around a noncanonical Watson – Crick base pair U13:G22:G46, is crucial for PUS7 activity, highlighting the correct, local spatial organization for catalysis [68]. In addition, yeast PUS7 was found to also catalyze Ψ_{35} and Ψ_{56} in U2 snRNA, although most other Ψs (e.g. Ψ_{34} in human or Ψ_{35} in yeast U2 snRNAs) are installed by the guide-RNA mediated H/ACA RNP [72,74]. Furthermore, PUS7 (like PUS1 and PUS4) is also responsible for Ψ-formation in mRNAs [8,9], which apparently is dynamically triggered in response to specific cellular stresses. Whether the recognition motifs for PUS7-dependent mRNA targets are the same as for tRNAs and how these recognition patterns are affected by cellular stress signalling will still require further investigations.

PUS10 is the only PUS enzyme exhibiting apparently redundant activity

PUS10 is a distinct member of the PUS superfamily as it is present in archaea and eukarya but absent in bacteria (Figure 1). Notably, its presence in fungi is also limited, with only 10 out of 50 fully sequenced fungal genomes encoding *pus10* genes [33]. The initial characterization of archaeal PUS10 activity

ribbon style (orange). In case of Pus1, one strand of RNA is from a non-functional interaction unit, which is highlighted in pink. Each Ψ sites and its responsible PUS are color coded, including rose for TruB (1K8W), light blue for TruA (Pus1, 7R9G; PUS3, 9ENE), purple for RluA (2I82). (B). A cartoon representative of a 23s rRNA molecule (9CL9) in the centre with large ribosomal subunits are shown with surface (grey) and RNA with ribbon style (orange). RluB is bound in this structure and is highlighted with surface mode (purple). Another example of RNA bound to RluF structure (3DH3) is presented where RluF is shown in purple. The human TERT H/ACA snoRNAP is also illustrated (right, 7TRC) with individual subunits colored and indicated. Close-up look at each binding site near the catalytic pocked of each PUS is illustrated. The PUS structure is same color code while the bound RNA is orange and nucleotides are shown with filled style. Forefingers (olive) and thumb (violet) fingers are highlighted and colored. The bound RNA secondary structures are shown in 2D cartoon style. The recognition consensus sequences are shown, and the target sites are as indicated with red triangles. In case of DKC1 complex, the unpaired dinucleotides of target RNA (cyan) are indicated as NΨ.

demonstrated its involvement in the formation of Ψ_{55} in archaeal tRNAs, serving as a functional orthologue for the PUS4/TruB-mediated modification, which is absent in archaea [75,76]. Subsequent studies on different PUS10 homologs carrying subtle sequence differences further revealed its capacity to modify either U_{54} and U_{55} (or both) in tRNAs (Figure 2A) [77,78]. In humans, PUS10 catalyzes the conversion of U_{54} to Ψ_{54} in a subset of tRNAs [26], whereas in other tRNAs U_{54} is universally modified to ribothymidine [64,79]. The selectivity depends on the presence of a conserved consensus sequence (GUUCAAAUC) around the U_{54} site [79]. In detail, the reported human PUS10-dependent tRNA targets [26,79] include $tRNA^{Cys}$, $tRNA^{Arg}$, $tRNA^{Pro}$, $tRNA^{Lys3}$, $tRNA^{Gln}$, $tRNA^{Trp}$, and $tRNA^{Thr}$. However, some of these apparent targets appear to lack the exact PUS10 consensus sequence motif. For instance, $tRNA^{Lys3}$ contains G_{59} instead the consensus A_{59}, and $tRNA^{Arg}$ carries G_{57} and C_{59} instead of the canonical A_{57} and A_{59}. Notably, the methylation at A_{58} position maximize PUS10 activity, demonstrating a cross-talk regulation of RNA modification at this region [79]. This seems to represent a unique regulatory feature of PUS10 comparing to other PUS enzyme that do not require any pre-requisite/priming modification in their proximty [26]. In addition, PUS10 can catalyze the formation of Ψ_{55} in tRNAs that do not contain the Ψ_{54}-dependent sequence motif [79], suggesting a degree of redundancy between the activities of PUS10 and TruB1/PUS4 [79]. Another study points out that the presence of a U_{54}·A_{58} reverse Hoogsteen pair is a crucial determinant for PUS10 activity, but not TruB1/PUS4, on Ψ_{55} formation in tRNAs [64].

To date, only the apo structure of human PUS10 has been reported [31], and no structural data is available for a PUS10 enzyme bound to a RNA substrate. The structure of the human PUS10 enzymes shares the common core topology with other members of the PUS superfamily and harbours a strictly conserved catalytic aspartic acid residue [31]. The THUMP domain of PUS10, located at the N-terminus, exhibits structural similarity to the THUMP domain of 4-thiouridine synthase ThiI from *Bacillus anthracis* [80] and has been implicated in RNA binding and recognition [76]. In addition, the THUMP domain in PUS10 contains a Zn-binding motif comprising four conserved cysteines, a feature distinct among PUS enzymes. Basic residues and Zn-coordinating cysteines within the THUMP domain, although distant from the catalytic site, are crucial for Ψ_{54} formation, but do not seem to be responsible PUS10-mediated Ψ_{55} modification.

RluA recognizes a RNA motif and a consensus sequence

In bacteria, RluA, RluC and RluD, belong to RluA superfamily of PUS enzymes (Figure 1), but they show unique substrate selectivity (Figure 2) [32,81]. RluC and RluD target-specific sites in 23s rRNA [30,81], including 955/2504/2580 for RluC and 1911/1915/1917 for RluD (Figure 2B). While RluD-dependent targets are consistently found within stem-loop motifs, the specific selection criteria for RluC have not been described, yet [81]. In contrast, RluA targets multiple RNA classes, including tRNA (U_{32}) (Figure 2A) and rRNA (U_{746}) (Figure 2B) [32]. Its target sites are embedded within a consensus sequence (ΨUNNAAA, where N represents any nucleotide) and are located in a stem-loop motif [32].

RluA, RluC and RluD have similar core structures, featuring an eight-stranded β-sheet [81–83] as well as a conserved architecture of the catalytic sites [84]. However, they show also several obvious structural differences. First, the surface potentials for the catalytic domains of RluC and RluD are very different. In detail, the opposite site of the catalytic cleft of RluC is positively charged and that of RluD is negatively charged [81]. Second, RluD contains a unique C-terminal helix that is highly negatively charged [81]. Third, the N-termini of RluA, RluC and RluD are different, and RluC and RluD both contain a S4-like RNA binding domain [81], which is absent in RluA. Of note, the structure of this S4-like RNA binding domain has not been visualized in any of the obtained electron density maps due to its intrinsic flexibility. Overall, these differences seem to contribute to how these PUS enzymes select and position their RNA substrates [84].

Several human PUS enzymes belong to the RluA superfamily, including RPUSD1, RPUSD2, RPUSD3, and RPUSD4. However, their activities, substrate specificity and target sites are not well characterized, like for the bacterial RluA homologs. Crystal structures of the enzymatic core region, as well as the flanking motifs, of RPUSD1 and RPUSD4 display a highly conserved topology (Table 1). However, mechanistic studies on these proteins remain elusive. Via an *in vitro* pseudouridine assignment approach, it was shown that human RPUSD2 shows pseudouridylation

activity towards mRNAs, but no consistent sequence contexts have been identified for the detected RPUSD2-dependent target sites [59]. It was shown in human cell lines that RPUSD3 and RPUSD4 (along with TRUB2) are part of a module that control mitochondrial 16s rRNA and mitochondrial protein synthesis [83]. Of note, RPUSD3 does not carry the conserved catalytic aspartic acid [85] and as it is considered a pseudoenzyme, the mechanisms of how it regulates rRNA maturation remains elusive. Human RPUSD4 has been shown to be active towards pre-mRNAs in an *in vitro* screen [86], but whether it also acts on mitochondrial pre-mRNA is not clear.

RluA was crystallized in complex with the anticodon stem loop of $tRNA^{Phe}$, revealing an extensive network of RluA–RNA interactions at the 5′-half of the bound hairpin [32,87] (Figure 2). The complex architecture resembles the recognition elements that are shared with RsuA and TruA [45]. However, RluA drastically rearranges the structure of the bound RNA molecule to facilitate probing the suitable substrate as part of its unique selection mechanism [32]. In detail, RluA reshapes the entire bound RNA structure, shifting it from a U-turn conformation to a reverse-Hoogsteen base pair. It flips out position U_{32}, G_{34}, and A_{37} from the helical stack of the stem-loop to also reposition A_{36}, which leads to the formation of a reverse-Hoogsteen base pair with the U_{33} base [32]. This substantial conformational rearrangement in the substrate allows the flipping of the target U_{32}, while the cationic guanidino group of an arginine residue at the catalytic site can intercalate between the newly formed reverse-Hoogsteen base pair to compensate and stabilize the flipped-out position. These drastic structural changes of the bound RNA also suggest a strong requirement of consensus sequence context (ΨUNNAAA) to accommodate the new base pair (U_{33}:A_{36}), defining A_{36} as a crucial determinant for substrate selection. Whether this mechanism can be applied to the human counterparts still needs to be confirmed.

RsuA superfamily specifically modify rRNA

RsuA, RluB, RluE and RluF belong to the RsuA superfamily of PUS enzymes, which is known to modify sites in 16S or 23S rRNAs (Figure 1) [82,88,89]. Members of this family have a similar structural arrangement like RluC and RluD, which harbour a N-terminal S4-like α3β4 domain that is connected via an extended linker region to the conserved core domain [82,90–92]. The linker allows the S4-like domain to undergo a hinge-mediated motion when binding to RNA substrates. The S4-like domain interacts with the major groove of RNA, pinning the bound RNA from one end, and positioning the loop containing the target site into the catalytic site [50,93]. It was shown that this domain in RsuA facilitates substrate recognition [93] and to target U_{516} in helix 18 of the 16S rRNA [82], which apparently is the only Ψ in this rRNA subunit [94]. RsuA preferably binds to the target site at an intermediate rRNA assembly state, exposing the otherwise inaccessible site for pseudouridylation [93]. RluE, like RsuA, targets a single uridine at position 2457, which is located in helix 89 of the 23S rRNA. This stringent substrate specificity is mediated via unique loops in the core region and in N-terminus that mediate sequence-specific contacts [89]. RluB and RluF modify U_{2605} and U_{2604} in 23S rRNA, respectively, but apparently RluF can occasionally also modify U_{2605} (Figure 2). They both recognize stem-loop motifs but display different modes of binding that explains their different selectivity. For instance, RluF rearranges the bound RNA by 'frame-shifting' the base-pairing pattern, inducing a bulge, in the stem-loop, which subsequently flips out the U_{2604} nucleotide [49,50]. When the bulge is removed by mutation, RluF shows strongly reduced modification activity for U_{2604}, highlighting the dependency on the induced structural element [49]. In contrast, RluB does not change the bound RNA structure and directly flips out U_{2605}. Of note, no RsuA homologs have been identified in archaea or eukaryotes, yet.

Conserved PUS catalytic mechanism with regulation variation

Prior to the actual isomerization reaction, target uridines located in folded RNA domains must undergo base flipping to enter the catalytic active site [32,36,45]. To understand these specific steps of PUS-mediated modification reactions, different strategies have been applied to structurally capture the intermediate states in PUS–RNA complex (Figure 3A,B). Two co-crystal structures of RsuA with uracil or UMP display these

non-polymerized RNA nucleotides in the catalytic sites in close proximity to the catalytic aspartic acid [91]. Several co-crystal structures of RNA bound to PUS enzymes, including RluB [50], TruB [36], or RluA [32], were obtained using RNA substrates that contained uridine analogs instead of the target U. In the case of the RluB/RNA complex a covalent bond was formed between 5-FU and a tyrosine residue in the active site, resulting in a fluoro-hydroxy-pseudouracil intermediate [50]. A similar strategy was applied to trap the RNA-TruA intermediate, where the target uridine was replaced with a non-target guanidine nucelotide [45]. This structure provides details of how the flipped-out nucleotide is secured in place without the formation of an artificial covalent adduct.

Comparing these available structures of PUS enzymes, including TruA/PUS3 [40,45], TruB [36], TruD [67], PUS10 [76], it becomes obvious that they all share a (at least partially) conserved architecture of active site during catalysis through an aspartate-arginine network [41], or aspartate-lysine network in the case of PUS10 and TruD (Figure 3). Foremost, flipping-out the target nucleotide seems to be a common mechanism in PUS-mediated catalysis, which is achieved via a common arginine residue located in the same loop as the catalytic Asp [32,45] to chelate and replace the target nucleotide (Figure 3). However, this residue is conserved only in TruA, RluA, RsuA, and PUS10. At the catalytic site, there are other several conserved residues to assist pseudouridinylation by stabilizing the flipped-out conformation of the nucleotide. In the case of TruB, the flipped-out 5FU at position 55 in tRNAs is stabilized by stacking interactions with Tyr76 and Tyr179 [36]. It is placed near the catalytic Asp48, which is further stabilized by Arg181 through a salt bridge. This salt bridge-mediated interaction may activate Asp48 for subsequent nucleophilic attack during pseudouridylation. A similar arrangement of these mentioned functional residues is also found in TruA, PUS3 and PUS10, where the two conserved aromatic tyrosine residues stack with the flipped-out nucleotide. In addition, a conserved basic residue (Arg in TruA, TruB and RsuA; Lys in RluA and PUS10) forms a stabilizing salt bridge with the catalytic Asp residue [45]. While the RNA-bound structure of TruA directly confirmed this mechanism, the role of these residues in PUS3 and PUS10 is inferred based on structural homology.

For all PUS enzymes, the catalytic cleft features a large, predominantly hydrophobic cavity, lined by hydrophobic residues (e.g. Val and Leu), which also seem to aid in positioning the flipped-out nucleotide within the active site [36,45]. Notably, TruB exhibits a more extensive RNA interaction surface [36] compared to TruA, which makes only a limited number of contacts with the ASL [40,45]. For instance, His43 of TruB stacks beneath the reverse Hoogsteen U_{54}:A_{58} base pair, which further stabilizes the formed complex and ensures site-specific recognition of U_{55} [36].

Comparative sequence analyses indicate the evolutionary divergence of TruD from other PUS enzymes. TruD exhibits minimal sequence similarity to other PUS families [71]. Moreover, several conserved residues in most PUS family members are replaced by different amino acids. For instance, the conserved arginine residue, which is crucial to form a salt-bridging [95] with the catalytic Asp in all other PUS family members, is replaced with a lysine in TruD [71] (within *E. coli* TruD) (Figure 3C). This Lys21 from a close-by loop region seems to interact with the Asp within the catalytic cleft. Furthermore, the stacking Tyr residue is replaced by Phe131 (within *E. coli* TruD), which could also stack with the target uracil. The supporting hydrophobic residues also differ between TruD and TruB where Phe27 substitutes for the Leu, and Ala330 replaces the Ile/Va in the binding site [71]. These variants indicate a structural and functional divergence, tailored to the substrate recognition and enzymatic activity of TruD.

Dyskerin DKC1 requires a guide RNA for site specific pseudouridylation

In contrast to the mechanisms by the stand-alone PUS enzymes, DKC1, belonging to TruB superfamily, not only utilizes its own accessory domain but also auxiliary proteins to accommodate a guide RNA (H/ACA snoRNA) to achieve site-specific pseudouridylation in archaea and eukaryotes (Figure 1) [47,96,97]. DKC1 RNP-dependent pseudouridylation activity is essential for rRNA processing and ribosome biogenesis [98], as well as for the maturation of spliceosomal small nuclear RNAs (snRNA), which is crucial for pre-mRNA splicing [99]. Of note, DKC1 homologs in archaea and yeast are named as Cbf5 and the first structural information about the complex has been obtained from an archaeal Cbf5 complex [100,101]. It shows an overall 'triangle shape' where the PUS enzyme Cbf5 sits in the centre as a hub that binds L7ae [a human non-histone protein 2 (NHP2) homolog], glycine–arginine-rich protein 1 (Gar1) and nucleolar protein 10 (Nop10). The Cbf5, containing a TruB domain followed by an archaeosine transglycosylase (PUA) domain,

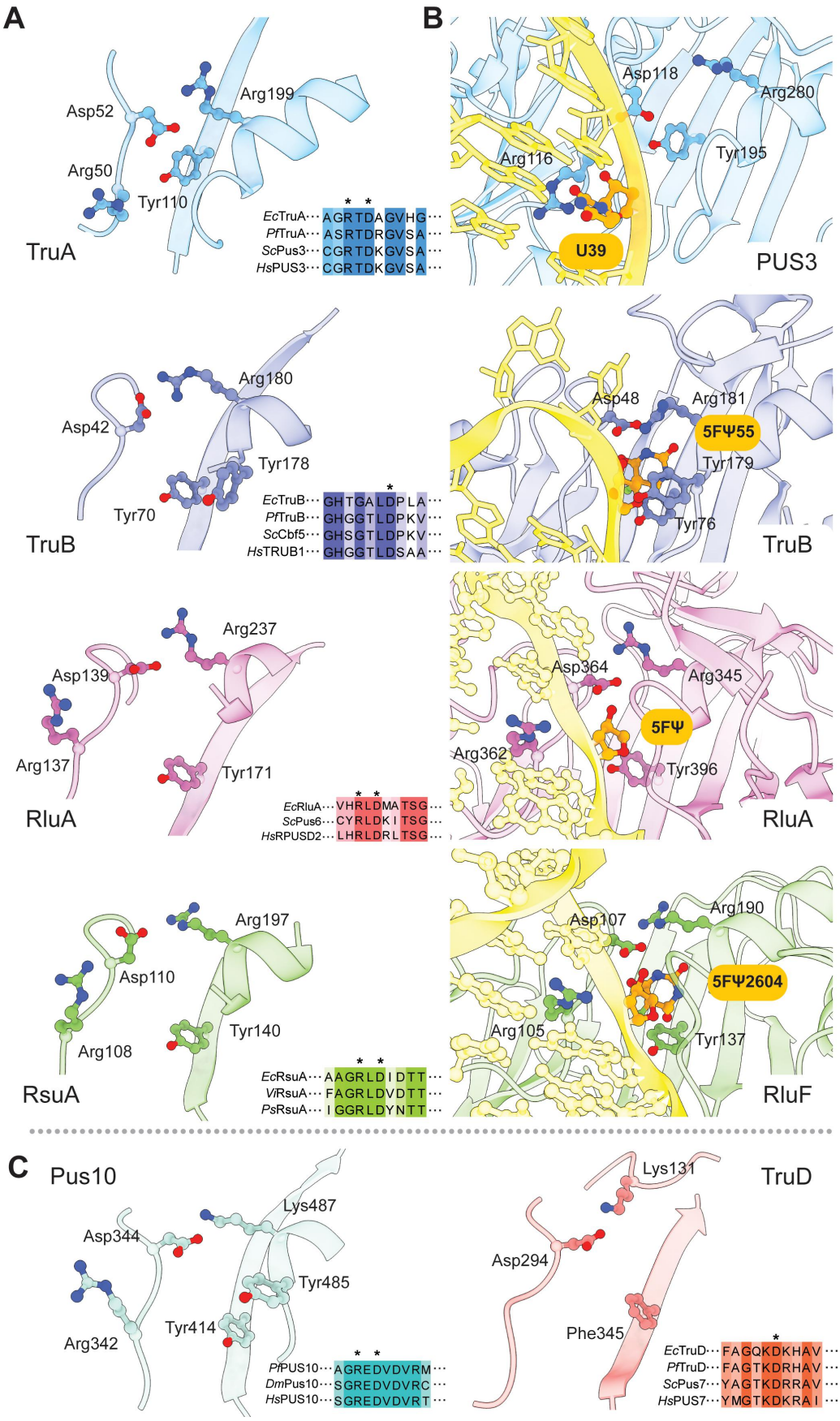

Figure 3. Close-up look at the catalytic sites with and without RNA bound. (A-B). Pair comparison of apo and RNA bound PUS at the catalytic pockets where each PUS is color-coded, including light blue for TruA (apo, 1VS3; bound, 8OKD); blue for

serves a platform for L7ae, NOP10 and Gar1 [101], stabilizing the hetero-tetramer. The complex components, except for Gar1, extensively interact with the snoRNA, which has a conserved H/ACA hairpin that adapts a near-linear secondary structure consisting of a K-turn motif and two helical stems that sandwich the 5′ and 3′ guide sequences (Figure 2). The guide sequences, forming a large internal loop, provide a pseudouridylation pocket to base-pair with targets residing in rRNAs and positioning them near the catalytic cleft of Cbf5. In detail, the 5′ guide sequence points away from Cbf5 and the 3′ guide sequence makes contacts with Cbf5. This large loop structure, without the presence of RNA substrate, remains highly flexible even when fully integrated into the Cbf5 complex, suggesting that this mobile structure can adopt numerous conformations before pairing with the target rRNA [101].

Human DKC1 shares a similar core structure with TruB family members, displaying a common PUS topology fold and a conserved catalytic aspartic acid located in a loop within the catalytic cleft [102]. However, eukaryotic DKC1 possess additional N-terminal and C-terminal extensions, which are absent in archaeal Cbf5. Interestingly, human DKC1 RNP is also found to be associated with telomerase complex (TERT) [103] (Figure 1), which binds to the chromosome telomeres and extends them by adding species specific repeat sequences. Recently, a few cryo-EM structures have revealed the molecular architecture of the telomerase H/ACA ribonucleoprotein [102,104], which is very similar to the archaeal counterpart. However, two copies of DKC1 H/ACA RNP bind to the double hairpin telomerase RNA where each tetramer interacts with one hairpin while the two tetramers interact with each other through each DKC1 subunit [102]. This inter-DKC1 interaction is essential for complex integrity, which is mediated via the N-terminal extension motif providing electrostatic and hydrophobic interactions [104].

The RNA substrate base-pairs with both, 5′ and 3′ guide sequences, and adopts a U-turn conformation while the UN dinucleotide (U, the target uridine; N, any nucleotide) remains unpaired and is located at the apex of the U-turn architecture, presenting it to the DKC1/Cbf5 catalytic site [105]. DKC1/Cbf5 harbours a thumb loop that can be a closed or open conformation for controlling the substrate turnover (Figure 2) [104]. The regulation of the loop is associated with GAR1, which senses the catalytic cycle during catalysis. However, how similar the catalytic mechanisms of the Cbf5 and the DKC1 complexes are, remains to be shown and will requires additional studies. Also, the exact role of the DKC1 H/ACA RNP and functional importance for telomerase activity is currently still under investigation.

Numerous genomic mutations in PUS enzymes are linked to human diseases

Over the past decade, clinical studies have identified mutations in PUS genes as causative factors in various human diseases, including severe neurodegenerative disorders. Although all PUS enzymes share the same fundamental pseudouridylation activity, their specificity for distinct sets of RNA targets result in different molecular and cellular consequences. Consequently, mutations in different PUS enzymes lead to diverse disease phenotypes, symptoms, and clinical outcomes. These unfortunate link to patients highlights the critical role of RNA modifications in maintaining cellular function and homoeostasis (Figure 4).

We would like to highlight an excellent review on the role of PUS enzymes in cancers [106]. Nonetheless, we surveyed the cancer genome atlas program that has collected single nucleotide polymorphism (SNP)-related data from patients' tissues spanning over 33 cancer types (TCGA Database). We found over 60 described missense mutations of PUS7 and PUS10 in affected tissues of cancer patients. The severity of each variant on the structure and function of PUS7 concerning cancer progression and severity can be assessed by the pathogenicity predictions using SIFT, PolyPhen and VEP tools [107,108]. However, further biochemical characterizations of each mutation should be performed to address if they are disease-causative factors.

TruB (apo, 1SGV; bound, 1K8W), purple for RluA (apo, 1QYU; bound, 2I82); green for RsuA (apo, 4LAB; bound, 3DH3). All bound RNA is colored yellow while the target uridine and uridine derivatives are shown in orange. (C). The catalytic sites of Pus10 (light cyan) and TruD (rose) are illustrated and color-coded. The universal catalytic aspartic residue as well as highly conserved residues are highlighted with balls and sticks style (red is oxygen, blue is nitrogen). The sequence conservation (generated using Jalview) around the catalytic aspartic residue of each PUS superfamily is shown in the insets where the D (aspartic acid) and R (arginine) are indicated with an asterisk. *Vi*: *Vibrio parahaemolyticus*; *Ps*: *Pseudomonas aeruginosa*; *Dm*: *Drosophila melanogaster*.

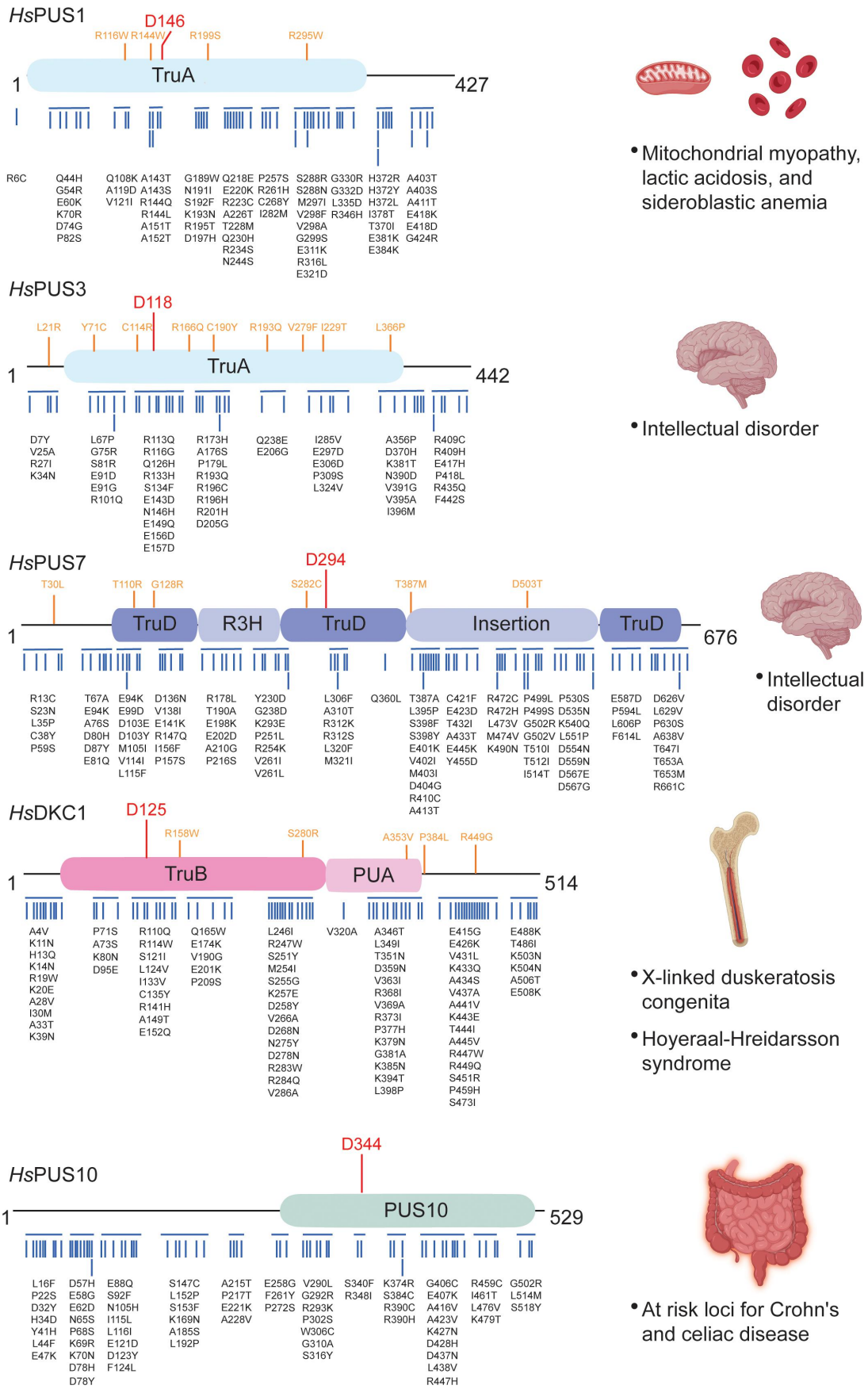

Figure 4. Summary of reported alterations of diseases relevant PUS. The residue numbers and domains of human PUS are indicated. The locations of the alterations are as listed in the cartoon representation. The catalytic aspartic acid residues are indicated with red, the alterations found in cancer samples are in black, and those for non-cancer diseases are in orange. Examples of non-cancer diseases for indicated PUS is shown on the right.

PUS1 and mitochondrial myopathy with lactic acidosis and sideroblastic anemia (MLASA)

Two isoforms (ENST00000376649.8 and ENST00000443358.6) encoded for human PUS1 were identified and they produce proteins of 427 and 399 amino acids, respectively [109]. The longer isoform contains a mitochondrial localization signal at the N-terminus, whereas the shorter isoform lacks the first 30 amino acids yet retains its pseudouridylation activity [40]. Mutations in the human *PUS1* gene are a causative factor in the rare autosomal recessive disorder mitochondrial myopathy and sideroblastic anaemia (MLASA) [110]. This condition is characterized by a significant deficiency in mitochondrial respiratory chain complexes I and IV, leading to impaired muscle strength and a range of additional symptoms, including chronic sideroblastic anaemia, diarrhoea, microcephaly, exercise intolerance, and growth retardation. Many MLASA cases arise from homozygous nonsense mutations in *PUS1*, such as Arg116Trp [110], Arg144Trp [111], Arg199Ser [112], Arg295Trp [113], or a frameshift mutation (Pro175fs) (Figure 5) [114]. Functional studies in a mouse model (Arg100Trp, equivalent to human Arg116Trp) confirm that these mutations result in a loss of PUS1 function [109]. Consequently, the absence of pseudouridylation in PUS1-dependent mitochondrial tRNAs [109] and mitochondrial mRNAs (e.g. *MTND4*) [40] disrupts mitochondrial protein synthesis. Of note, loss of PUS1 activity also disrupts the pseudouridine profiles in certain cytosolic tRNAs [109]. All changes may ultimately contribute to impaired erythropoiesis [109] and MLASA pathogenesis. Recently, a c.579-580insT truncated pathogenic variant was identified in the *PUS1* gene (MIM 608,109) in two patients with congenital sideroblastic anaemia. Although alterations in mtDNA copy number were found in patient cells, the detailed mechanistic link between PUS1 function and the clinical observations awaits confirmation [115].

PUS3 and intellectual disorders with wide spectrum of associated symptoms

Several clinical cases of a rare autosomal recessive neurodevelopmental disorder have been associated with homozygous or compound heterozygous variants in the *PUS3* gene [54,116–120]. These *PUS3* variants include single amino acid substitutions, nonsense mutations, splice variants, and nucleotide substitutions in the start codon. Patients carrying PUS3 mutations present global severe developmental delays, epileptic seizures, and additional symptoms such as renal disorders. Functional studies on clinically relevant PUS3 missense mutations, including Leu21Arg, Cys114Arg, Arg166Gln, Cys190Tyr, Arg193Gln, Val279Phe, Leu366Pro, and the Arg435 (c.1303C > T) frameshift mutation*—have been performed using patient-derived fibroblasts and *in vitro* biochemical assays (Figure 5) [40,116]. These analyses confirm that the loss of PUS3 function can arise through different routes, including abolished protein expression, reduced stability, impaired tRNA binding, or loss of enzymatic activity [40,54]. As PUS3 specifically catalyzes pseudouridylation in tRNAs, its loss is expected to have a broad impact on tRNA-mediated protein translation, contributing to the observed neurodevelopmental abnormalities.

PUS7 and intellectual diseases and cancers

Several clinical studies, which performed whole genome sequencing on material from patient who suffer from neurodevelopmental disorders, identified disease-relevant mutations in PUS7 [121–126]. Patients carrying clinical *PUS7* variants present similar phenotypes to intellectually disabled patients with *PUS3* mutations. Some of these clinically relevant PUS7 variants have been functionally characterized, including Thr30Lys, Arg450 (c.1348C > T) frameshift mutation*, Thr110Arg, and Asp503Tyr (Figure 5) [122,123]. Similar to PUS3 clinical variants, these analyses indicate loss-of-function of PUS7 and lower levels of Ψ_{13} on tRNAs. The reduced modification leads to impaired protein translation of specific transcripts, leading to neurodevelopmental delay [125]. Recently, different studies focused on the mechanistic link between PUS7 and the development of glioblastoma [127], colorectal cancer [128,129] and other cancer types. First, PUS7 seems to be overexpressed in cancerous tissues compared to healthy tissues [127–134]. The elevated expression levels are correlated with poor cancer prognosis, late disease progression, tumorigenesis and an increased metastatic potential. Of note, the overexpression of PUS7 leads to aberrant or abnormal profiles of pseudouridylation of tRNAs and mRNA transcripts [127]. These changes likely lead to

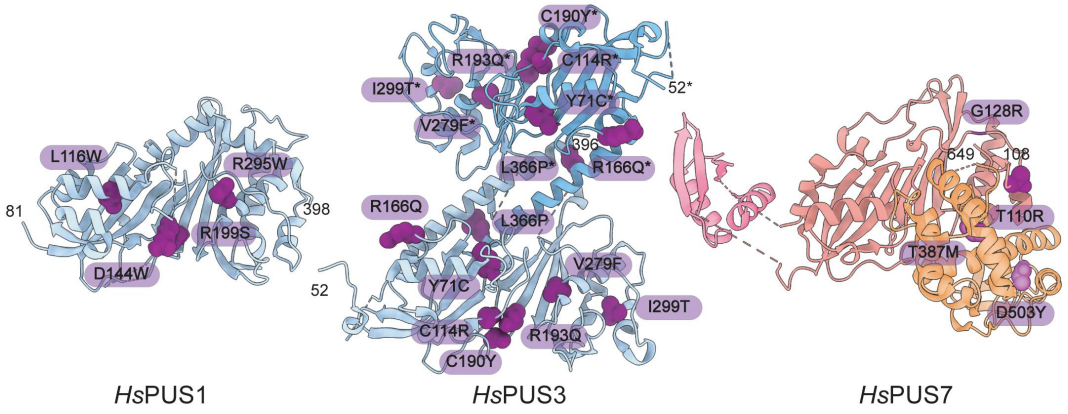

Figure 5. Examples of clinically relevant mutations found in human PUS. Cartoon illustrations of human PUS1 (left, PDB 4J37), PUS3 (middle, PDB 9F9Q) and PUS7 (right, PDB 5KKP) structures. The reported mutations linked to intellectual disorders or MASLA are highlighted in purple sphere. For clarity, the accessory domains of PUS7 is colored in pink and orange. The N-ter and C-ter residue positions of each PUS structure are indicated.

the stabilization of certain sets of mRNAs by reducing the rate of degradation, as well as, increasing the translation efficiency of transcripts that promote cancer migration and progression. Strikingly, some other studies find the opposite correlation, were reduced levels of PUS7 expression are linked to cancer progression and migration [135–137]. For instance, a PUS7-dependent pseudouridylation at the U_{696} position of alpha-ketoglutarate-dependent dioxygenase alkB Homolog 3 (ALKBH3) mRNAs was found to act as a tumour suppressor in human gastric cancer tissues. Therefore, reduced PUS7 expression hampers the translation of ALHBH3 mRNA, promoting gastric cancer progression and tumorigenesis [135]. Hence, cellular PUS7 levels (as well as its modification activity) need to be kept in balance to avoid negative consequences on human health.

PUS10 and diseases

Similar to PUS7, different studies have also linked PUS10 expression and mutants to cancer (TCGA Database). However, only few studies explore the mechanistic link between PUS10 and cancer in greater detail. Biochemical analyses have primarily found low expression of PUS10 to be linked to poor prognosis, tumorigenesis, metastasis and progression in various cancers. A cell-based study has shown that reducing the modification levels of $\Psi_{54/55}$ in tRNAs diminishes cell viability, indicating that PUS10 is crucial for cell survival [138]. Interestingly, the same study reports that PUS10 can bind to the so called microprocessor complex, namely DGCR8 and DROSHA. However, this function of PUS10 that supports pre-miRNA processing and miRNA biogenesis does not require its pseudouridylation activity. Another study supporting this mechanism shows that PUS10 promotes the maturation of miR-194-5p, which is crucial to avoid metastasis of renal cell carcinoma [139].

DKC1 and diseases

Pathogenic mutations in human DKC1 have been linked to X-linked dyskeratosis congenita (X-DC) [140,141] and Hoyeraal-Hreidarsson syndrome (HHS) [142], both of which predominantly affect males [143]. X-DC is a rare disorder with skin abnormalities and bone marrow failure that leads to premature death while HHS is a severe form of X-DC. Many patients diagnosed with X-DC carried a recurring missense mutation, Ala353Val [140], along with other mutations [144], such as Arg158Trp, Ser280Arg and Pro384Leu. To date, many clinical cases of X-DC continue to be reported, with newly identified pathogenic mutations in DKC1 and other components of the DKC1 RNP complex and telomere complex [143,145]. These pathogenic DKC1 mutations are frequently found in the PUA domain, disrupting RNA interactions, impairing telomerase RNA binding and ribosome assembly [104]. Some mutations occur in the N-terminal

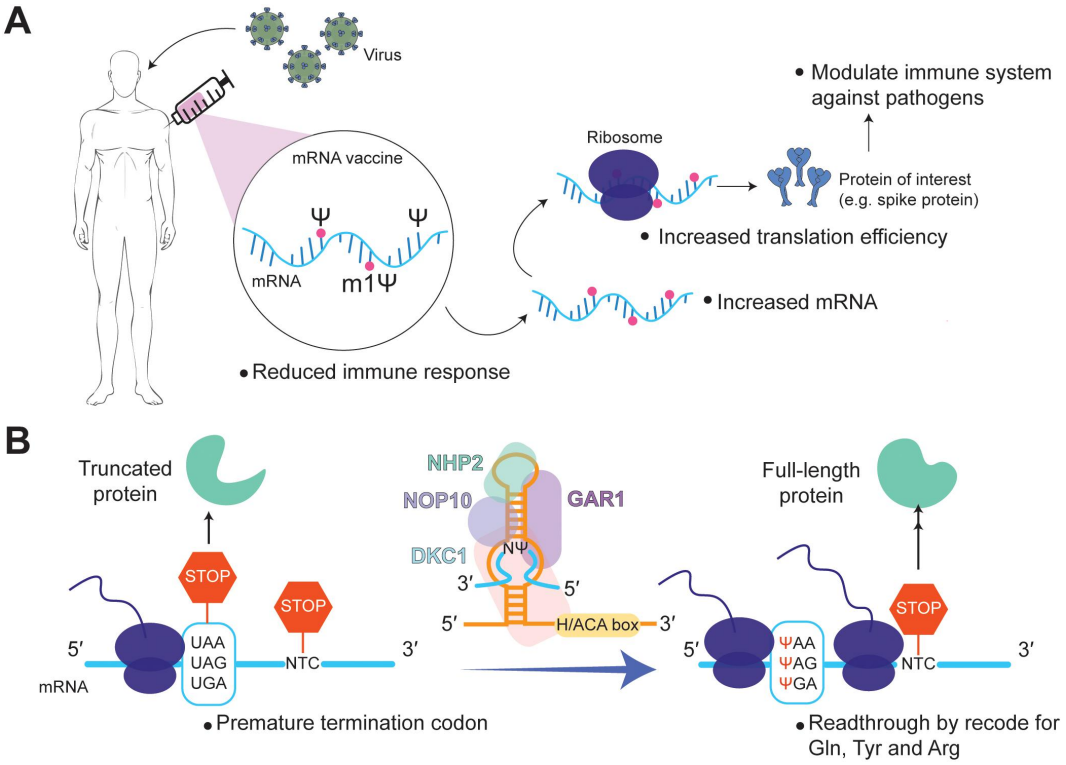

Figure 6. Examples of Ψ in biomedical applications. (A). A diagram of mRNA vaccine with implemented Ψ to help with reduced immune response against synthetic mRNA that carries information for producing target proteins. Ψ also helps with increasing synthetic mRNA stability and translation efficiency. (B). A scheme of programmable pseudouridylation via DKC1 complex to convert the uridines at the premature termination codon to Ψ, which allows the ribosome to readthrough by recoding it for glutamine, tyrosine or arginine residues and produces full-length proteins.

extension of DKC1, weakening the inter-DKC1 interface within the telomerase complex, while others are located in the C-terminal extension (amino acids 381–417), where the nuclear localization signal is present. A study on patient-derived induced pluripotent stem cells carrying mutations in this region displays shortened telomere length [146]. Additionally, DKC1 undergoes post-translational SUMOylation at Lys39 and Lys43, and mutations at these residues are also linked to X-DC, suggesting that post-translational modifications are essential for DKC1 stability [147]. Mutations at the DKC1-NOP10 interface have also been identified as causative factors for X-DC, leading to telomere attrition [148].

Conclusion and future aspect on pseudouridylation

The discovery of numerous Ψ-sites in coding RNAs suggests a regulatory role in transcript stability and protein synthesis, increasing interest in its biological significance. In addition, the introduction of Ψ (or derivatives [149] thereof) into synthetic mRNAs has enhanced the efficiency of mRNA vaccines by providing stabilization while at the same time also reducing immune responses when admitted to mice (Figure 6A) [150,151].

While RNA sequencing technologies have advanced pseudouridine mapping across the transcriptome [16], accurate site verification remains a challenge due to limitations in detection sensitivity and transcript abundance [40]. Moreover, the shape and flexibility of RNA can affect the ability of PUS enzymes to modify their target sites. Since RNA folds into complex secondary and tertiary structures, some uridine nucleotides may be buried within stable regions, making them inaccessible to PUS enzymes under certain conditions. The structures of many RNAs are dynamic, meaning they can change conformations in response to cellular conditions [152]. If a pseudouridylation site is only transiently exposed, it may be difficult to detect using standard high throughput sequencing

or biochemical methods. This structural variability may explain why some predicted Ψ-sites are not always modified or detectable in different cellular contexts.

Emerging cryo-EM studies are expected to provide high-resolution insights into PUS-RNA interactions, offering a structural basis for pseudouridylation site selection and regulation. Integrating these structural insights with transcriptome-wide mapping will refine our understanding of Ψ's role in RNA metabolism. For instance, a recent advance in biomedical applications using DKC1-mediated site-specific pseudouridinylation provides a potential solution to tackling premature termination codon [153] (Figure 6B). RNA structure determination is not governed by a single type of modification – instead, multiple modifications work in regulatory harmony to locally modulate structural dynamics by influencing RNA modification patterns [154]. To date, a small portion of such crosstalk between different RNA modifications has been identified (see reviews [155,156], and its underlying mechanisms remain largely unexplored. Therefore, these advances will not only expand fundamental knowledge of functional interpretation of Ψ for RNA biology, but also support synthetic RNA biology, enabling precise RNA modification strategies for biotechnology and therapeutic applications [150,153].

Disclosure statement

No potential conflict of interest was reported by the author(s).

Funding

Research funding for this study was provided by European Research Council (ERC) under the European Union's Horizon 2020 research and innovation program grant No [101001394] (SG).

ORCID

Ting-Yu Lin http://orcid.org/0000-0001-7914-2164
Sebastian Glatt http://orcid.org/0000-0003-2815-7133

CRediT author statement

Ting-Yu Lin: Conceptualization, Supervision, Visualization, Writing – original draft, Writing – review & editing. **Yasmin Stone**: Visualization, Writing – original draft, Writing – review & editing. **Sebastian Glatt**: Conceptualization, Funding acquisition, Supervision, Visualization, Writing – original draft, Writing – review & editing

Data availability statement

No data was generated in this work.

References

[1] Boccaletto P, Stefaniak F, Ray A, et al. Modomics: a database of RNA modification pathways. 2021 update. Nucleic Acids Res. 2021;50(D1):D231–D235. doi: 10.1093/nar/gkab1083
[2] Shi H, Chai P, Jia R, et al. Novel insight into the regulatory roles of diverse RNA modifications: re-defining the bridge between transcription and translation. Mol Cancer. 2020;19(1). doi: 10.1186/s12943-020-01194-6
[3] Jonkhout N, Tran J, Smith MA, et al. The RNA modification landscape in human disease. RNA. 2017;23(12):1754–1769. doi: 10.1261/rna.063503.117
[4] Gu X, Liu Y, Santi DV. The mechanism of pseudouridine synthase I as deduced from its interaction with 5-fluorouracil-tRNA. Proc Natl Acad Sci USA. 1999;96(25):14270–14275. doi: 10.1073/pnas.96.25.14270
[5] Begik O, Lucas MC, Pryszcz LP, et al. Quantitative profiling of pseudouridylation dynamics in native RNAs with nanopore sequencing. Nat Biotechnol. 2021;39(10):1278–1291. doi: 10.1038/s41587-021-00915-6
[6] Addepalli B, Limbach PA. Mass spectrometry-based quantification of pseudouridine in RNA. J Am Soc Mass Spectrom. 2011;22(8):1363–1372. doi: 10.1007/s13361-011-0137-5

[7] Hermon SJ, Sennikova A, Becker S. Quantitative detection of pseudouridine in RNA by mass spectrometry. Sci Rep. 2024;14(1):27564. doi: 10.1038/s41598-024-78734-3
[8] Carlile TM, Rojas-Duran MF, Zinshteyn B, et al. Pseudouridine profiling reveals regulated mRNA pseudouridylation in yeast and human cells. Nature. 2014;515(7525):143–146. doi: 10.1038/nature13802
[9] Dai Q, Zhang LS, Sun HL, et al. Quantitative sequencing using BID-seq uncovers abundant pseudouridines in mammalian mRNA at base resolution. Nat Biotechnol. 2022;41(3):344–354. doi: 10.1038/s41587-022-01505-w
[10] Marchand V, Pichot F, Neybecker P, et al. HydraPsiSeq: a method for systematic and quantitative mapping of pseudouridines in RNA. Nucleic Acids Res. 2020;48(19):e110–e110. doi: 10.1093/nar/gkaa769
[11] Campos CM, Tsai K, Courtney DG, et al. Mapping of pseudouridine residues on cellular and viral transcripts using a novel antibody-based technique. RNA. 2021;27(11):1400–1411. doi: 10.1261/rna.078940.121
[12] Zhang W, Eckwahl MJ, Zhou KI, et al. Sensitive and quantitative probing of pseudouridine modification in mRNA and long noncoding RNA. RNA. 2019;25(9):1218–1225. doi: 10.1261/rna.072124.119
[13] Xu H, Kong L, Cheng J, et al. Absolute quantitative and base-resolution sequencing reveals comprehensive landscape of pseudouridine across the human transcriptome. Nat Methods. 2024;21(11):2024–2033. doi: 10.1038/s41592-024-02439-8
[14] Zhang N, Shi S, Jia TZ, et al. A general LC-MS-based RNA sequencing method for direct analysis of multiple-base modifications in RNA mixtures. Nucleic Acids Res. 2019;47(20):E125–E125. doi: 10.1093/nar/gkz731
[15] Rodell R, Robalin N, Martinez NM. Why U matters: detection and functions of pseudouridine modifications in mRNAs. Trends Biochem Sci. 2024;49(1):12–27. doi: 10.1016/j.tibs.2023.10.008
[16] Gilbert WV. Recent developments, opportunities, and challenges in the study of mRNA pseudouridylation. RNA. 2024;30(5):530–536. doi: 10.1261/rna.079975.124
[17] Lin TY, Mehta R, Glatt S. Pseudouridines in RNAs: switching atoms means shifting paradigms. FEBS Lett. 2021;595(18):2310–2322. doi: 10.1002/1873-3468.14188
[18] Helm M, Schmidt-Dengler MC, Weber M, et al. General principles for the detection of modified nucleotides in RNA by specific reagents. Adv Biol. 2021;5(10). doi: 10.1002/adbi.202100866
[19] Motorin Y, Helm M. General principles and limitations for detection of RNA modifications by sequencing. Acc Chem Res. 2024;57(3):275–288. doi: 10.1021/acs.accounts.3c00529
[20] Owens MC, Zhang C, Liu KF. Recent technical advances in the study of nucleic acid modifications. Mol Cell. 2021;81(20):4116–4136. doi: 10.1016/j.molcel.2021.07.036
[21] Cerneckis J, Ming GL, Song H, et al. The rise of epitranscriptomics: recent developments and future directions. Trends Pharmacol Sci. 2024;45(1):24–38. doi: 10.1016/j.tips.2023.11.002
[22] van der Feltz C, DeHaven AC, Hoskins AA. Stress-induced pseudouridylation alters the structural equilibrium of yeast U2 snRNA stem II. J Mol Biol. 2018;430(4):524–536. doi: 10.1016/j.jmb.2017.10.021
[23] Ding J, Bansal M, Cao Y, et al. Myc drives mRNA pseudouridylation to mitigate proliferation-induced cellular stress during cancer development. Cancer Res. 2024;84(23):4031–4048. doi: 10.1158/0008-5472.CAN-24-1102
[24] Rajan KS, Adler K, Doniger T, et al. Identification and functional implications of pseudouridine RNA modification on small noncoding RNAs in the mammalian pathogen Trypanosoma brucei. J Biol Chem. 2022;298(7):298. doi: 10.1016/j.jbc.2022.102141
[25] Sharma S, Woodworth B, Yang B, et al. Quantitative mapping of pseudouridines in bacteria RNA. BioRxiv. 2024.
[26] Biela AD, Nowak JS, Biela AP, et al. Determining the effects of pseudouridine incorporation on human tRNAs. EMBO J. 2025;44(13):3553–3585. doi: 10.1038/s44318-025-00443-y
[27] Sloan KE, Warda AS, Sharma S, et al. Tuning the ribosome: the influence of rRNA modification on eukaryotic ribosome biogenesis and function. RNA Biol. 2017;14(9):1138–1152. doi: 10.1080/15476286.2016.1259781
[28] Zhao Y, Rai J, Yu H, et al. CryoEM structures of pseudouridine-free ribosome suggest impacts of chemical modifications on ribosome conformations. Structure. 2022;30(7):983–992.e5. doi: 10.1016/j.str.2022.04.002
[29] Wu G, Adachi H, Ge J, et al. Pseudouridines in U2 snRNA stimulate the ATPase activity of Prp5 during spliceosome assembly. EMBO J. 2016;35(6):654–667. doi: 10.15252/embj.201593113
[30] Hamma T, Ferré-D'Amaré AR. Pseudouridine synthases. Chem Biol. 2006;13(11):1125–1135. doi: 10.1016/j.chembiol.2006.09.009
[31] McCleverty CJ, Hornsby M, Spraggon G, et al. Crystal structure of human Pus10, a novel pseudouridine synthase. J Mol Biol. 2007;373(5):1243–1254. doi: 10.1016/j.jmb.2007.08.053
[32] Hoang C, Chen J, Vizthum CA, et al. Crystal structure of pseudouridine synthase RluA: indirect sequence readout through protein-induced RNA structure. Mol Cell. 2006;24(4):535–545. doi: 10.1016/j.molcel.2006.09.017
[33] Fitzek E, Joardar A, Gupta R, et al. Evolution of eukaryal and archaeal pseudouridine synthase Pus10. J Mol Evol. 2018;86(1):77–89. doi: 10.1007/s00239-018-9827-y
[34] Veerareddygari GR, Singh SK, Mueller EG. The pseudouridine synthases proceed through a glycal intermediate. J Am Chem Soc. 2016;138(25):7852–7855. doi: 10.1021/jacs.6b04491
[35] Dong X, Bessho Y, Shibata R, et al. Crystal structure of the tRNA pseudouridine synthase TruA from Thermus thermophilus HB8. RNA Biol. 2006;3(3):115–121. doi: 10.4161/rna.3.3.3286
[36] Hoang C, Ferré -D'amaré AR. Cocrystal structure of a tRNA 55 pseudouridine synthase: nucleotide flipping by an RNA-modifying enzyme. Cell. 2001;107(7):929–939. doi: 10.1016/S0092-8674(01)00618-3

[37] Spedaliere CJ, Ginter JM, Johnston MV, et al. The pseudouridine synthases: revisiting a mechanism that seemed settled. J Am Chem Soc. 2004;126(40):12758–12759. doi: 10.1021/ja046375s
[38] Miracco EJ, Mueller EG. The products of 5-fluorouridine by the action of the pseudouridine synthase Trub disfavor one mechanism and suggest another. J Am Chem Soc. 2011;133(31):11826–11829. doi: 10.1021/ja201179f
[39] Kiss DJ, Oláh J, Tóth G, et al. The structure-derived mechanism of box H/ACA pseudouridine synthase offers a plausible paradigm for programmable RNA editing. ACS Catal. 2022;12(5):2756–2769. doi: 10.1021/acscatal.1c04870
[40] Lin TY, Kleemann L, Jeżowski J, et al. The molecular basis of tRNA selectivity by human pseudouridine synthase 3. Mol Cell. 2024;84(13):2472–2489.e8. doi: 10.1016/j.molcel.2024.06.013
[41] Friedt J, Leavens FMV, Mercier E, et al. An arginine-aspartate network in the active site of bacterial TruB is critical for catalyzing pseudouridine formation. Nucleic Acids Res. 2014;42(6):3857–3870. doi: 10.1093/nar/gkt1331
[42] Kaya Y, Del Campo M, Ofengand J, et al. Crystal structure of TruD, a novel pseudouridine synthase with a new protein fold. J Biol Chem. 2004;279(18):18107–18110. doi: 10.1074/jbc.C400072200
[43] Safra M, Nir R, Farouq D, et al. Trub1 is the predominant pseudouridine synthase acting on mammalian mRNA via a predictable and conserved code. Genome Res. 2017;27(3):393–406. doi: 10.1101/gr.207613.116
[44] Pan H, Agarwalla S, Moustakas DT, et al. Structure of tRNA pseudouridine synthase TruB and its RNA complex: rNA recognition through a combination of rigid docking and induced fit. Proc Natl Acad Sci USA. 2003;100(22):12648–12653. doi: 10.1073/pnas.2135585100
[45] Hur S, Stroud RM. How U38, 39, and 40 of many tRNAs become the targets for pseudouridylation by TruA. Mol Cell. 2007;26(2):189–203. doi: 10.1016/j.molcel.2007.02.027
[46] Ganot P, Bortolin M-L, Kiss T. Site-specific pseudouridine formation in preribosomal RNA is guided by small nucleolar RNAs. Cell. 1997;89(5):799–809. doi: 10.1016/S0092-8674(00)80263-9
[47] Lafontaine DLJ, Cile bousquet-Antonelli C, Henry Y, et al. The box H+ACA snoRNAs carry Cbf5p, the putative rRNA pseudouridine synthase. Gene Devel. 1998;12(4):527–537. doi: 10.1101/gad.12.4.527
[48] Grünberg S, Doyle LA, Wolf EJ, et al. The structural basis of mRNA recognition and binding by yeast pseudouridine synthase PUS1. PLOS ONE. 2023;18(11):e0291267. doi: 10.1371/journal.pone.0291267
[49] Alian A, DeGiovanni A, Griner SL, et al. Crystal structure of an RluF-RNA complex: a base-pair rearrangement is the key to selectivity of RluF for U2604 of the ribosome. J Mol Biol. 2009;388(4):785–800. doi: 10.1016/j.jmb.2009.03.029
[50] Czudnochowski N, Ashley GW, Santi DV, et al. The mechanism of pseudouridine synthases from a covalent complex with RNA, and alternate specificity for U2605 versus U2604 between close homologs. Nucleic Acids Res. 2014;42(3):2037–2048. doi: 10.1093/nar/gkt1050
[51] Foster PG, Huang L, Stroud DV, et al. The structural basis for tRNA recognition and pseudouridine formation by pseudouridine synthase I. Nat Struct Biol. 2000;7(1):23–27. doi: 10.1038/71219
[52] Sibert BS, Fischel-Ghodsian N, Patton JR. Partial activity is seen with many substitutions of highly conserved active site residues in human pseudouridine synthase 1. RNA. 2008;14(9):1895–1906. doi: 10.1261/rna.984508
[53] Blaby IK, Majumder M, Chatterjee K, et al. Pseudouridine formation in archaeal RNAs: the case of Haloferax volcanii. RNA. 2011;17(7):1367–1380. doi: 10.1261/rna.2712811
[54] Lin TY, Smigiel R, Kuzniewska B, et al. Destabilization of mutated human PUS3 protein causes intellectual disability. Hum Mutat. 2022;43(12):2063–2078. doi: 10.1002/humu.24471
[55] Arena F, Ciliberto G, Ciampi S, et al. Purification of pseudouridylate synthetase I from Salmonella typhimurium. Nucleic Acids Res. 1978;5(12):4523–4536. doi: 10.1093/nar/5.12.4523
[56] Schweke H, Pacesa M, Levin T, et al. An atlas of protein homo-oligomerization across domains of life. Cell. 2024;187(4):999–1010.e15. doi: 10.1016/j.cell.2024.01.022
[57] Schaening-Burgos C, G-W L, Gilbert W, et al. Rlua is the major mRNA pseudouridine synthase in *Escherichia coli*. PLoS Genet. 2024;20(9):e1011100. doi: 10.1371/journal.pgen.1011100
[58] Czudnochowski N, Wang AL, Finer-Moore J, et al. In human pseudouridine synthase 1 (hPus1), a C-terminal helical insert blocks tRNA from binding in the same orientation as in the Pus1 bacterial homologue TruA, consistent with their different target selectivities. J Mol Biol. 2013;425(20):3875–3887. doi: 10.1016/j.jmb.2013.05.014
[59] Carlile TM, Martinez NM, Schaening C, et al. mRNA structure determines modification by pseudouridine synthase 1. Nat Chem Biol. 2019;15(10):966–974. doi: 10.1038/s41589-019-0353-z
[60] Becker HF, Motorin Y, Planta RJ, et al. The yeast gene YNL292w encodes a pseudouridine synthase (Pus4) catalyzing the formation of Ψ 55 in both mitochondrial and cytoplasmic tRNAs. Nucleic Acids Res. 1997;25(22):4493–4499. doi: 10.1093/nar/25.22.4493
[61] Nurse K, Wrzensinski J, Bakin A, et al. Purification, cloning, and properties of the tRNA psi 55 synthase from Escherichia coli. RNA. 1995;1(1):102–112.
[62] Jia Z, Meng F, Chen H, et al. Human TRUB1 is a highly conserved pseudouridine synthase responsible for the formation of ψ55 in mitochondrial tRNA*asn*, tRNA*gln*, tRNA*glu* and tRNA*pro*. Nucleic Acids Res. 2022;50(16):9368–9381. doi: 10.1093/nar/gkac698

[63] Gu X, Yu M, Ivanetich KM, et al. Molecular recognition of tRNA by tRNA pseudouridine 55 synthase. Biochemistry. 1998;37(1):339–343. doi: 10.1021/bi971590p
[64] Mukhopadhyay S, Deogharia M, Gupta R. Mammalian nuclear TRUB1, mitochondrial TRUB2, and cytoplasmic PUS10 produce conserved pseudouridine 55 in different sets of tRNA. RNA. 2021;27(1):66–79. doi: 10.1261/rna.076810.120
[65] Schultz SKL, Kothe U. tRNA elbow modifications affect the tRNA pseudouridine synthase TruB and the methyltransferase TrmA. RNA. 2020;26(9):1131–1142. doi: 10.1261/rna.075473.120
[66] Tavakoli S, Nabizadeh M, Makhamreh A, et al. Semi-quantitative detection of pseudouridine modifications and type I/II hypermodifications in human mRNAs using direct long-read sequencing. Nat Commun. 2023;14(1):14. doi: 10.1038/s41467-023-35858-w
[67] Kaya Y, Ofengand J. A novel unanticipated type of pseudouridine synthase with homologs in bacteria, archaea, and eukarya. RNA. 2003;9(6):711–721. doi: 10.1261/rna.5230603
[68] Guegueniat J, Halabelian L, Zeng H, et al. The human pseudouridine synthase PUS7 recognizes RNA with an extended multi-domain binding surface. Nucleic Acids Res. 2021;49(20):11810–11822. doi: 10.1093/nar/gkab934
[69] Ericsson UB, Nordlund P, Hallberg BM. X-ray structure of tRNA pseudouridine synthase TruD reveals an inserted domain with a novel fold. FEBS Lett. 2004;565(1–3):59–64. doi: 10.1016/j.febslet.2004.03.085
[70] Purchal MK, Eyler DE, Tardu M, et al. Pseudouridine synthase 7 is an opportunistic enzyme that binds and modifies substrates with diverse sequences and structures. Proc Natl Acad Sci USA. 2022;119(4):e2109708119. doi: 10.1073/pnas.2109708119
[71] Hoang C, Ferré-D'Amaré AR. Crystal structure of the highly divergent pseudouridine synthase TruD reveals a circular permutation of a conserved fold. RNA. 2004;10(7):1026–1033. doi: 10.1261/rna.7240504
[72] Behm-Ansmant I, Urban A, Ma X, et al. The Saccharomyces cerevisiae U2 snRNA: pseudouridine-synthase Pus7p is a novel multisite-multisubstrate RNA: ψ-synthase also acting on tRNAs. RNA. 2003;9(11):1371–1382. doi: 10.1261/rna.5520403
[73] Ma X, Zhao X, Y-T Y. Pseudouridylation (ψ) of U2 snRNA in S. cerevisiae is catalyzed by an RNA independent mechanism. EMBO J. 2003;22(8):1889–1897. doi: 10.1093/emboj/cdg191
[74] Wu G, Xiao M, Yang C, et al. U2 snRNA is inducibly pseudouridylated at novel sites by Pus7p and snR81 RNP. Embo J. 2011;30(1):79–89. doi: 10.1038/emboj.2010.316
[75] Roovers M, Droogmans L, Grosjean H. Post-transcriptional modifications of conserved nucleotides in the T-loop of tRNA: a tale of functional convergent evolution. Genes (Basel). 2021;12(2):1–19. doi: 10.3390/genes12020140
[76] Kamalampeta R, Keffer-Wilkes LC, Kothe U. Trna binding, positioning, and modification by the pseudouridine synthase Pus10. J Mol Biol. 2013;425(20):3863–3874. doi: 10.1016/j.jmb.2013.05.022
[77] Gurha P, Gupta R. Archaeal Pus10 proteins can produce both pseudouridine 54 and 55 in tRNA. RNA. 2008;14(12):2521–2527. doi: 10.1261/rna.1276508
[78] Li Y, Wu S, Ye K. Landscape of RNA pseudouridylation in archaeon Sulfolobus islandicus. Nucleic Acids Res. 2024;52(8):4644–4658. doi: 10.1093/nar/gkae096
[79] Deogharia M, Mukhopadhyay S, Joardar A, et al. The human ortholog of archaeal Pus10 produces pseudouridine 54 in select tRNAs where its recognition sequence contains a modified residue. RNA. 2019;25(3):336–351. doi: 10.1261/rna.068114.118
[80] Waterman DG, Ortiz-Lombardía M, Fogg MJ, et al. Crystal structure of Bacillus anthracis ThiI, a tRNA-modifying enzyme containing the predicted RNA-binding THUMP domain. J Mol Biol. 2006;356(1):97–110. doi: 10.1016/j.jmb.2005.11.013
[81] Mizutani K, Machida Y, Unzai S, et al. Crystal structures of the catalytic domains of pseudouridine synthases RluC and RluD from Escherichia coli. Biochemistry. 2004;43(15):4454–4463. doi: 10.1021/bi036079c
[82] Wrzesinski J, Bakin A, Nurse K, et al. Purification, cloning, and properties of the 16S RNA pseudouridine 516 synthase from Escherichia coli. Biochemistry. 1995;34(27):8904–8913. doi: 10.1021/bi00027a043
[83] Arroyo JD, Jourdain AA, Calvo SE, et al. A genome-wide CRISPR death screen identifies genes essential for oxidative phosphorylation. Cell Metab. 2016;24(6):875–885. doi: 10.1016/j.cmet.2016.08.017
[84] Spedaliere CJ, Hamilton CS, Mueller EG. Functional importance of motif I of pseudouridine synthases: mutagenesis of aligned lysine and proline residues. Biochemistry. 2000;39(31):9459–9465. doi: 10.1021/bi001079n
[85] Borchardt EK, Martinez NM, Gilbert WV. Regulation and function of RNA pseudouridylation in human cells. Annu Rev Genet. 2020;54(1):309–336. doi: 10.1146/annurev-genet-112618-043830
[86] Martinez NM, Su A, Burns MC, et al. Pseudouridine synthases modify human pre-mRNA co-transcriptionally and affect pre-mRNA processing. Mol Cell. 2022;82(3):645–659.e9. doi: 10.1016/j.molcel.2021.12.023
[87] Hamilton CS, Greco TM, Vizthum CA, et al. Mechanistic investigations of the pseudouridine synthase RluA using RNA containing 5-fluorouridine. Biochemistry. 2006;45(39):12029–12038. doi: 10.1021/bi061293x
[88] Del Campo M, Kaya Y, Ofengand J. Identification and site of action of the remaining four putative pseudouridine synthases in Escherichia coli. 2001.
[89] Tillault AS, Schultz SK, Wieden HJ, et al. Molecular determinants for 23S rRNA recognition and modification by the E. coli pseudouridine synthase RluE. J Mol Biol. 2018;430(9):1284–1294. doi: 10.1016/j.jmb.2018.03.011

[90] Matte A, Louie GV, Sivaraman J, et al. Structure of the pseudouridine synthase RsuA from Haemophilus influenzae. Acta Crystallogr Sect F Struct Biol Cryst Commun. 2005;61(4):350–354. doi: 10.1107/S1744309105005920
[91] Sivaraman J, Sauvé V, Larocque R, et al. Structure of the 16S rRNA pseudouridine synthase RsuA bound to uracil and UMP. Nat Struct Biol. 2002;9:353–358. doi: 10.1038/nsb788
[92] Sunita S, Zhenxing H, Swaathi J, et al. Domain organization and crystal structure of the catalytic domain of E. coli RluF, a pseudouridine synthase that acts on 23S rRNA. J Mol Biol. 2006;359(4):998–1009. doi: 10.1016/j.jmb.2006.04.019
[93] Jayalath K, Frisbie S, To M, et al. Pseudouridine synthase Rsua captures an assembly intermediate that is stabilized by ribosomal protein S17. Biomolecules. 2020;10(6):10. doi: 10.3390/biom10060841
[94] Bakin A, Ofengand J. Four newly located pseudouridylate residues in Escherichia coli 23S ribosomal RNA are all at the peptidyltransferase center: analysis by the application of a new sequencing technique. Biochemistry. 1993;32(37):9754–9762. doi: 10.1021/bi00088a030
[95] Hoang C, Hamilton CS, Mueller GE, et al. Precursor complex structure of pseudouridine synthase TruB suggests coupling of active site perturbations to an RNA-sequestering peripheral protein domain. Protein Sci. 2005;14(8):2201–2206. doi: 10.1110/ps.051493605
[96] Henras A, Henry Y, Cile bousquet-Antonelli C, et al. Nhp2p and Nop10p are essential for the function of H/ACA snoRnps. Embo J. 1998;17(23):7078–7090. doi: 10.1093/emboj/17.23.7078
[97] Normand C, Capeyrou R, Quevillon-Cheruel S, et al. Analysis of the binding of the N-terminal conserved domain of yeast Cbf5p to a box H/ACA snoRNA. RNA. 2006;12(10):1868–1882. doi: 10.1261/rna.141206
[98] Garus A, Autexier C. Dyskerin: an essential pseudouridine synthase with multifaceted roles in ribosome biogenesis, splicing, and telomere maintenance. RNA. 2021;27(12):1441–1458. doi: 10.1261/rna.078953.121
[99] Zhao Y, Karijolich J, Glaunsinger B, et al. Pseudouridylation of 7 SK sn RNA promotes 7 SK sn RNP formation to suppress HIV -1 transcription and escape from latency. EMBO Rep. 2016;17(10):1441–1451. doi: 10.15252/embr.201642682
[100] Rashid R, Liang B, Baker DL, et al. Crystal structure of a Cbf5-Nop10-Gar1 complex and implications in RNA-guided pseudouridylation and dyskeratosis congenita. Mol Cell. 2006;21(2):249–260. doi: 10.1016/j.molcel.2005.11.017
[101] Li L, Ye K. Crystal structure of an H/ACA box ribonucleoprotein particle. Nature. 2006;443(7109):302–307. doi: 10.1038/nature05151
[102] Nguyen THD, Tam J, Wu RA, et al. Cryo-EM structure of substrate-bound human telomerase holoenzyme. Nature. 2018;557(7704):190–195. doi: 10.1038/s41586-018-0062-x
[103] Mitchell JR, Wood E, Collins K. A telomerase component is defective in the human disease dyskeratosis congenita. Nature. 1999;402(6761):551–555. doi: 10.1038/990141
[104] Ghanim GE, Sekne Z, Balch S, et al. 2.7 Å cryo-EM structure of human telomerase H/ACA ribonucleoprotein. Nat Commun. 2024;15(1):15. doi: 10.1038/s41467-024-45002-x
[105] Wu H, Feigon J, Dickerson RE. H/aca small nucleolar RNA pseudouridylation pockets bind substrate RNA to form three-way junctions that position the target U for modification. Proc Natl Acad Sci USA. 2007;104(16):6655–6660. doi: 10.1073/pnas.0701534104
[106] Liu K, Zhang S, Liu Y, et al. Advancements in pseudouridine modifying enzyme and cancer. Front Cell Dev Biol. 2024;12:12. doi: 10.3389/fcell.2024.1465546
[107] Adzhubei IA, Schmidt S, Peshkin L, et al. A method and server for predicting damaging missense mutations. Nat Methods. 2010;7(4):248–249. doi: 10.1038/nmeth0410-248
[108] Kumar P, Henikoff S, Ng PC. Predicting the effects of coding non-synonymous variants on protein function using the SIFT algorithm. Nat Protoc. 2009;4(7):1073–1081. doi: 10.1038/nprot.2009.86
[109] Shi D, Wang B, Li H, et al. Pseudouridine synthase 1 regulates erythropoiesis via transfer RNAs pseudouridylation and cytoplasmic translation. iScience. 2024;27(3):27. doi: 10.1016/j.isci.2024.109265
[110] Bykhovskaya Y, Casas K, Mengesha E, et al. Missense mutation in pseudouridine synthase 1 (PUS1) causes mitochondrial myopathy and sideroblastic anemia (MLASA). Am J Hum Genet. 2004;74(6):1303–1308. doi: 10.1086/421530
[111] Kothari SS, Shah J, Sharma V, et al. Severe pulmonary arterial hypertension in congenital sideroblastic anemia from PUS1 mutation – a case report. BMC Med Genomics. 2024;17(1):17. doi: 10.1186/s12920-024-01983-8
[112] Xiong Y, Yang W, Fan H, et al. Myopathy with lactic acidosis and sideroblastic anemia caused by a novel PUS1 mutation. Blood. 2023;142(Supplement 1):5242–5242. doi: 10.1182/blood-2023-182770
[113] Metodiev MD, Assouline Z, Landrieu P, et al. Unusual clinical expression and long survival of a pseudouridylate synthase (PUS1) mutation into adulthood. Eur J Hum Genet. 2015;23(6):880–882. doi: 10.1038/ejhg.2014.192
[114] Wang B, Shi D, Yang S, et al. Mitochondrial tRNA pseudouridylation governs erythropoiesis. Blood. 2024;144(6):657–671. doi: 10.1182/blood.2023022004
[115] Ammar M, Kmiha S, Maalej M, et al. Identification of a novel truncated pathogenic variant in PUS1 gene in two siblings of consanguineous Tunisian family: intrafamilial phenotypic variability related to mtDNA copy number. Ann Hematol. 2025;104(2):943–952. doi: 10.1007/s00277-025-06259-4

[116] Shaheen R, Han L, Faqeih E, et al. A homozygous truncating mutation in PUS3 expands the role of tRNA modification in normal cognition. Hum Genet. 2016;135(7):707–713. doi: 10.1007/s00439-016-1665-7
[117] Nøstvik M, Kateta SM, Schönewolf-Greulich B, et al. Clinical and molecular delineation of PUS3-associated neurodevelopmental disorders. Clin Genet. 2021;100(5):628–633. doi: 10.1111/cge.14051
[118] Abdelrahman HA, Am A-S, Ali BR, et al. A null variant in PUS3 confirms its involvement in intellectual disability and further delineates the associated neurodevelopmental disease. Clin Genet. 2018;94(6):586–587. doi: 10.1111/cge.13443
[119] Fang H, Zhang L, Xiao B, et al. Compound heterozygous mutations in PUS3 gene identified in a Chinese infant with severe epileptic encephalopathy and multiple malformations. Neurol Sci. 2020;41(2):465–467. doi: 10.1007/s10072-019-04049-1
[120] De Paiva ARB, Lynch DS, Melo US, et al. PUS3 mutations are associated with intellectual disability, leukoencephalopathy, and nephropathy. Neurol Genet. 2019;5(1):e306. doi: 10.1212/NXG.0000000000000306
[121] de Brouwer APM, Abou Jamra R, Körtel N, et al. Variants in PUS7 cause intellectual disability with speech delay, microcephaly, short stature, and aggressive behavior. Am J Hum Genet. 2018;103(6):1045–1052. doi: 10.1016/j.ajhg.2018.10.026
[122] Darvish H, Azcona LJ, Alehabib E, et al. A novel PUS7 mutation causes intellectual disability with autistic and aggressive behaviors. Neurol Genet. 5(4): e356. doi: 10.1212/NXG.0000000000000356
[123] Shaheen R, Tasak M, Maddirevula S, et al. PUS7 mutations impair pseudouridylation in humans and cause intellectual disability and microcephaly. Hum Genet. 2019;138(3):231–239. doi: 10.1007/s00439-019-01980-3
[124] Muda A, Malerba L, Giordano L, et al. A PUS7 gene pathogenic variant causing self-injurious behavior, sleep disturbances, and developmental delay: a case report. Am J Med Genet A. 2023;191(7):1953–1958. doi: 10.1002/ajmg.a.63212
[125] Han ST, Kim AC, Garcia K, et al. PUS7 deficiency in human patients causes profound neurodevelopmental phenotype by dysregulating protein translation. Mol Genet Metab. 2022;135(3):221–229. doi: 10.1016/j.ymgme.2022.01.103
[126] Naseer MI, Abdulkareem AA, Jan MM, et al. Next generation sequencing reveals novel homozygous frameshift in PUS7 and splice acceptor variants in AASS gene leading to intellectual disability, developmental delay, dysmorphic feature and microcephaly. Saudi J Biol Sci. 2020;27(11):3125–3131. doi: 10.1016/j.sjbs.2020.09.033
[127] Cui Q, Yin K, Zhang X, et al. Targeting PUS7 suppresses tRNA pseudouridylation and glioblastoma tumorigenesis. Nat Cancer. 2021;2(9):932–949. doi: 10.1038/s43018-021-00238-0
[128] Song D, Guo M, Xu S, et al. Hsp90-dependent PUS7 overexpression facilitates the metastasis of colorectal cancer cells by regulating LASP1 abundance. J Exp Clin Cancer Res. 2021;40(1):170. doi: 10.1186/s13046-021-01951-5
[129] Zhang Q, Fei S, Zhao Y, et al. PUS7 promotes the proliferation of colorectal cancer cells by directly stabilizing SIRT1 to activate the Wnt/β-catenin pathway. Mol Carcinog. 2023;62(2):160–173. doi: 10.1002/mc.23473
[130] Du J, Gong A, Zhao X, et al. Pseudouridylate synthase 7 promotes cell proliferation and invasion in colon cancer through activating PI3K/AKT/mTOR signaling pathway. Dig Dis Sci. 2022;67(4):1260–1270. doi: 10.1007/s10620-021-06936-0
[131] Li H, Chen L, Han Y, et al. The identification of RNA modification gene PUS7 as a potential biomarker of ovarian cancer. Biology (basel). 2021;10(11):1130. doi: 10.3390/biology10111130
[132] Dong B, Wang B, Fan M, et al. Comprehensive analysis to identify PUS7 as a prognostic biomarker from pan-cancer analysis to osteosarcoma validation. Aging (Albany NY). 2024;16(10):9188–9203. doi: 10.18632/aging.205863
[133] Mohl DA, Lagies S, Zodel K, et al. Integrated metabolomic and transcriptomic analysis of modified nucleosides for biomarker discovery in clear cell renal cell carcinoma. Cells. 2023;12(8):12. doi: 10.3390/cells12081102
[134] Jin Z, Song M, Wang J, et al. Integrative multiomics evaluation reveals the importance of pseudouridine synthases in hepatocellular carcinoma. Front Genet. 2022;13. doi: 10.3389/fgene.2022.944681
[135] Chang Y, Jin H, Cui Y, et al. PUS7-dependent pseudouridylation of ALKBH3 mRNA inhibits gastric cancer progression. Clin Transl Med. 2024;14(8):14. doi: 10.1002/ctm2.1811
[136] Guzzi N, Cieśla M, Ngoc PCT, et al. Pseudouridylation of tRNA-derived fragments steers translational control in stem cells. Cell. 2018;173(5):1204–1216.e26. doi: 10.1016/j.cell.2018.03.008
[137] Wang X, Gao H, Pu W, et al. Dysregulation of pseudouridylation in small RNAs contributes to papillary thyroid carcinoma metastasis. Cancer Cell Int. 2024;24(1):24. doi: 10.1186/s12935-024-03482-3
[138] Song J, Zhuang Y, Zhu C, et al. Differential roles of human PUS10 in miRNA processing and tRNA pseudouridylation. Nat Chem Biol. 2020;16(2):160–169. doi: 10.1038/s41589-019-0420-5
[139] Luo W, Xu Z, Wang H, et al. HIF1A-repressed PUS10 regulates NUDC/Cofilin1 dependent renal cell carcinoma migration by promoting the maturation of miR-194-5p. Cell Biosci. 2023;13(1). doi: 10.1186/s13578-023-01094-4
[140] Knight SW, Heiss NS, Vulliamy TJ, et al. X-linked dyskeratosis congenita is predominantly caused by missense mutations in the DKC1 gene. Am J Hum Genet. 1999;65(1):50–58. doi: 10.1086/302446
[141] Vulliamy T, Marrone A, Goldman F, et al. The RNA component of telomerase is mutated in autosomal dominant dyskeratosis congenita. Nature. 2001;413(6854):432–435. doi: 10.1038/35096585
[142] Yaghmai R, Kimyai-Asadi A, Rostamiani K, et al. Overlap of dyskeratosis congenita with the Hoyeraal-Hreidarsson syndrome. J Pediatr. 2000;136(3):390–393. doi: 10.1067/mpd.2000.104295

[143] Neri Morales C, Cuestas D, Ángel F, et al. Dyskeratosis congenita associated with a novel missense variant in TERT: approach for the dermatologists. Arch Dermatol Res. 2024;316(7). doi: 10.1007/s00403-024-03050-9
[144] Knight SW, Vulliamy TJ, Morgan B, et al. Identification of novel DKC1 mutations in patients with dyskeratosis congenita: implications for pathophysiology and diagnosis. Hum Genet. 2001;108(4):299–303. doi: 10.1007/s004390100494
[145] Ratnasamy V, Navaneethakrishnan S, Sirisena ND, et al. Dyskeratosis congenita with a novel genetic variant in the DKC1 gene: a case report. BMC Med Genet. 2018;19(1). doi: 10.1186/s12881-018-0584-y
[146] Chu CM, Yu HH, Kao TL, et al. A missense variant in the nuclear localization signal of DKC1 causes Hoyeraal-Hreidarsson syndrome. NPJ Genom Med. 2022;7(1). doi: 10.1038/s41525-022-00335-8
[147] Brault ME, Lauzon C, Autexier C. Dyskeratosis congenita mutations in dyskerin SUMOylation consensus sites lead to impaired telomerase RNA accumulation and telomere defects. Hum Mol Genet. 2013;22(17):3498–3507. doi: 10.1093/hmg/ddt204
[148] Balogh E, Chandler JC, Varga M, et al. Pseudouridylation defect due to DKC1 and NOP10 mutations causes nephrotic syndrome with cataracts, hearing impairment, and enterocolitis. Proc Natl Acad Sci USA. 2020;117(26):15137–15147. doi: 10.1073/pnas.2002328117
[149] Monroe J, Eyler DE, Mitchell L, et al. N1-methylpseudouridine and pseudouridine modifications modulate mRNA decoding during translation. Nat Commun. 2024;15(1):8119. doi: 10.1038/s41467-024-51301-0
[150] Morais P, Adachi H, Yu YT. The critical contribution of pseudouridine to mRNA COVID-19 vaccines. Front Cell Dev Biol. 2021;9. doi: 10.3389/fcell.2021.789427
[151] Karikó K, Muramatsu H, Welsh FA, et al. Incorporation of pseudouridine into mRNA yields superior non-immunogenic vector with increased translational capacity and biological stability. Mol Ther. 2008;16(11):1833–1840. doi: 10.1038/mt.2008.200
[152] Cao X, Zhang Y, Ding Y, et al. Identification of RNA structures and their roles in RNA functions. Nat Rev Mol Cell Biol. 2024;25(10):784–801. doi: 10.1038/s41580-024-00748-6
[153] Song J, Dong L, Sun H, et al. Crispr-free, programmable RNA pseudouridylation to suppress premature termination codons. Mol Cell. 2023;83(1):139–155.e9. doi: 10.1016/j.molcel.2022.11.011
[154] Lucas MC, Pryszcz LP, Medina R, et al. Quantitative analysis of tRNA abundance and modifications by nanopore RNA sequencing. Nat Biotechnol. 2024;42(1):72–86. doi: 10.1038/s41587-023-01743-6
[155] Rengaraj P, Obrdlík A, Vukić D, et al. Interplays of different types of epitranscriptomic mRNA modifications. RNA Biol. 2021;18(sup1):19–30. doi: 10.1080/15476286.2021.1969113
[156] Sokołowski M, Klassen R, Bruch A, et al. Cooperativity between different tRNA modifications and their modification pathways. Biochim et Biophys Acta (BBA) - Gene Regul Mech. 2018;1861(4):409–418. doi: 10.1016/j.bbagrm.2017.12.003